Midmantle deformation between the Australian continent and the Fiji-Tonga subduction zone?

Maggy Heintz[1]

Received 19 September 2005; revised 4 April 2006; accepted 10 May 2006; published 8 September 2006.

[1] Shear wave splitting measurements are performed at temporary stations deployed across the Australian continent for direct S waves from events occurring in the neighboring subduction zones, especially Fiji-Tonga. Unlike core refracted shear waves, direct S waves are not polarized at the core-mantle boundary and are therefore subject to influences on the source side, on the receiver side, and along the ray path in between. Source side contamination due to the development of lattice preferred orientation of olivine can be minimized by considering deep events with an epicentral location below 410 km depth, the olivine-spinel phase transition depth. Anisotropic contributions from the transition zone or lower mantle can only be reliably inferred in the case of high delays that cannot be generated solely by the upper mantle structure underneath a station. The analysis of a comprehensive data set for direct S waves from deep events leads to an average delay time of 0.9 s at stations deployed across the continent. Despite the limitations of such an arithmetic average, the result highlights the lack of evidence for midmantle deformation between the Fiji-Tonga subduction zone and the Australian continent, unlike previously suggested in studies dealing with the permanent seismological stations only. A striking consistency between measurements performed across several stations belonging to an array in western Australia suggests a very coherent lithospheric structure underneath the Yilgarn craton.

Citation: Heintz, M. (2006), Midmantle deformation between the Australian continent and the Fiji-Tonga subduction zone?, *J. Geophys. Res.*, *111*, B09303, doi:10.1029/2005JB004058.

1. Introduction

[2] Seismic anisotropy, the variation of seismic wave velocity with respect to the propagation direction, is now a well developed tool for investigating the dynamics of the deep Earth processes. If an incoming polarized S wave encounters an anisotropic medium, it is split into two quasi S waves with perpendicular polarization that propagate with different velocities. The orientation of the fast S wave, phi, is assumed to be a proxy for the orientation of the crystallographic axes of anisotropic minerals in the upper mantle, mainly olivine. The delay between the arrival time of the fast and slow S components, dt, gives hints about the intrinsic anisotropy, the thickness of the anisotropic layer, the orientation of the ray path with respect to the elastic tensor of the anisotropic medium and the vertical coherence of the anisotropic fabric. Comparison of the anisotropic parameters measured at a seismological station with the absolute plate motion (APM) or the superficial tectonic trend, can therefore help understanding mantle flow and/or mechanical coupling between the crust and the upper mantle in a way that cannot be achieved by other geophysical methods.

[3] Over the last decade, seismic anisotropy has been extensively studied, particularly in continental areas. Seismic anisotropy appears to be constrained to the first 200 km of the upper mantle and has been attributed to the development of lattice preferred orientation (LPO) of olivine, the most abundant and deformable mineral in the first 410 km of the mantle. Evidence for seismic anisotropy at greater depth is limited (see *Silver* [1996] and *Savage* [1999] for review): the amount of anisotropy appears to be small in the transition zone and near the 660 km discontinuity [*Savage*, 1999], but some contributions from the D″ layer have been highlighted [*Kendall and Silver*, 1996]. The presence of anisotropy in the mid-low mantle region can also not be completely ruled out, and, for instance, a recent study [*Wookey and Kendall*, 2004; *Wookey et al.*, 2002] suggested a non negligible anisotropy in the uppermost lower mantle beneath the eastern part of the Australian plate.

[4] Splitting measurements are commonly performed on core refracted shear waves such as SK(K)S or PK(K)S. The P-to-S conversion at the core-mantle boundary (CMB) requires these phases to be radially polarized when they enter the mantle and any source side contamination is avoided. The angle of incidence at the seismological station is nearly vertical, and anisotropy measured at the Earth's surface therefore represents a vertically integrated effect of anisotropy from the CMB to the surface. All these advantages make core refracted shear waves a very popular tool for studying mantle anisotropy. These phases are distinct for

[1]Research School of Earth Sciences, Australian National University, Canberra, ACT, Australia.

0148-0227/06/2005JB004058$09.00

events occurring between 85 and 145° epicentral distance and show a good signal-to-noise ratio for magnitudes greater than 5.5 Mb. However, the average time span of recording of temporary networks is usually too short to allow the selection of enough events fulfilling the distance and magnitude criteria.

[5] An alternative approach to the study of mantle anisotropy is the use of direct S waves; the selection criteria for such direct S waves are also the epicentral distance (24–80°) and magnitude (greater than 5.5 Mb). Direct S waves are more energetic than core refracted shear waves, hence easier to identify on seismograms and leading to a potentially larger data set. Unlike core refracted shear waves, direct S waves are not polarized at the CMB and so are subject to influence of anisotropy located on the source side as well as on the ray path between the epicenter and the seismological station. It is a difficult exercise to dissociate the source side from the receiver side component in the measured anisotropic parameters. On the source side, anisotropy can be linked to the olivine LPO in the upper mantle and to the intrinsic composition of a subducting slab. A reliable way to remove any contamination from the source side is to select events occurring below the olivine-spinel phase transition, i.e., below 410 km depth. Upper mantle anisotropy can result in up to ~2 s of delay time, 1 s being the worldwide average for lithospheric anisotropy [*Silver*, 1996]. If unusually high delay times are measured, other sources of anisotropy have to be considered and possible contributions from the transition zone or the lower mantle, depending on the ray path of the wave, should be taken into account.

[6] The geographical location of Australia with respect to subduction zones, together with the dense continental coverage of temporary seismological stations reached by continuing efforts from the Research School of Earth Sciences, Australian National University, represent an ideal context for seismic anisotropy studies. Several studies dealing with core refracted shear wave splitting in Australia suggest apparent isotropy underneath the permanent stations [*Barruol and Hoffmann*, 1999; *Ozalaybey and Chen*, 1999; *Vinnik et al.*, 1992]. Considering the lack of splitting observed at the permanent stations over several years of recording, authors tend to consider the Australian upper mantle as isotropic. However, with the limited number of permanent stations across the continent, the assumption of an isotropic upper mantle may well be overstated. Measurements performed on direct S waves from deep events occurring in the Fiji-Tonga-Kermadec subduction zone recorded at the permanent stations display nonnegligible splitting values [*Wookey and Kendall*, 2004; *Wookey et al.*, 2002]. We therefore need to find a way to reconcile the lack of anisotropy from core refracted phases and the anisotropy in direct S waves intriguingly measured at the permanent stations [*Wookey and Kendall*, 2004; *Wookey et al.*, 2002].

[7] On the other hand, studies dealing with core refracted phases recorded over 6 months in average at stations deployed within the framework of the various temporary networks indicate some correlations with superficial structures [*Clitheroe and van der Hilst*, 1997; *Heintz and Kennett*, 2005], whereas 2 years of data analysis at the TASMAL stations in eastern Australia seem to highlight isotropy underneath numerous seismological stations [*Heintz and Kennett*, 2006].

[8] This paper presents shear wave splitting measurements performed on direct S waves from events occurring within the subduction zones surrounding Australia, with particular emphasis on the Fiji-Tonga subduction zone. The recordings are taken from the seismological stations temporarily deployed all over the continent. The aim of the study is to investigate (1) the possibility for midmantle deformation between Fiji-Tonga and the continent, as recently suggested [*Wookey and Kendall*, 2004; *Wookey et al.*, 2002], and (2) the existence of a vertically oriented transversely isotropic medium to reconcile the lack of SK(K)S phase splitting and the distinct direct S splitting.

2. Context of the Study and Previous Results

2.1. Receiver Side

[9] The Australian continent has experienced a long and complex tectonic evolution over the last 4.6 Gyr, involving the accretion and collision of various cratonic blocks previously part of large continental landmasses that may have included North America, East Antarctica, and greater India [*Betts et al.*, 2002; *Myers et al.*, 1996]. This complex tectonic history involving the lithosphere in its entire thickness may have left some imprints on the lithospheric structure. To some extent, these imprints can be recovered by geophysical techniques such as tomography, resulting in snapshots of the internal structure of the continent at various depths.

[10] Despite the various tomographic procedures used, the different models produced for the Australian upper mantle [*Debayle and Kennett*, 2000b; *Fishwick et al.*, 2005; *Kennett et al.*, 2004b; *Simons et al.*, 1999] all show a very strong contrast in seismic shear wave speeds between eastern and western Australia, along ~140°E longitude, and from 75 to at least 200 km depth. At a crustal scale, studies initially based on the separation of geological outcrops [*Hill*, 1951] and, more recently, on gravity and magnetic anomalies [*Gunn et al.*, 1997; *Scheibner*, 1974; *Shaw et al.*, 1996; *Veevers and Powell*, 1984], drew a boundary between western Precambrian and eastern Phanerozoic Australia, referred to as the "Tasman line" (TL). The concept of the TL remains highly controversial, with various authors suggesting various locations. The recent review of *Direen and Crawford* [2003] concluded that the TL may result from a number of sources that vary in age, protolith and degree of deformation/metamorphism; in this view, there is no basis for the interpretation of a coherent supracrustal Tasman "line" in the strictest sense. The contrast in shear wave speeds highlighted by surface wave tomography (subsequently referred to as the "tomographic TL") cannot be directly superimposed on any of the locations of the TL suggested by the previous studies. It rather corresponds to a mix, at depth, of the various definitions [*Kennett et al.*, 2004b]. The geodynamical implication of this feature however requires a definite separation between the geological evolution of western and eastern Australia.

[11] On the Australian continent, several studies have dealt with shear wave splitting analysis performed at the permanent stations [*Barruol and Hoffmann*, 1999; *Ozalaybey and Chen*, 1999; *Vinnik et al.*, 1992; *Wookey*

and Kendall, 2004; *Wookey et al.*, 2002], and at stations deployed within the first three stages of the SKIPPY experiment [*Clitheroe and van der Hilst*, 1997], an itinerant deployment of 10 broadband stations for a ~6 month period, resulting in the coverage of the whole continent within 3 years.

[12] The results from core refracted shear waves recorded at the permanent stations [*Barruol and Hoffmann*, 1999; *Ozalaybey and Chen*, 1999; *Vinnik et al.*, 1992; *Wookey and Kendall*, 2004; *Wookey et al.*, 2002] agree on the absence of receiver side splitting underneath the Australian stations, whereas high values of splitting (up to 7.1 s) are measured on direct S waves from the Fiji-Tonga subduction zone and recorded at the same permanent stations [*Wookey and Kendall*, 2004; *Wookey et al.*, 2002]. Considering the location of these five stations spread all over the continent (Figure 1), no conclusion can be drawn as to whether the lithosphere at the continental scale is anisotropic or not. Vertically oriented anisotropy would result in splitting from horizontally traveling direct S waves, but no splitting in core refracted shear waves because they are polarized in the radial-vertical plane by the P-to-S conversion at the CMB. *Clitheroe and van der Hilst* [1997] on the other hand, highlighted polarization directions in eastern Australia, from core refracted shear waves, exhibiting a curvilinear trend similar to that of the TL. Anisotropy frozen in the lithosphere is therefore not ruled out.

[13] A recent study [*Heintz and Kennett*, 2005] reported core refracted shear wave splitting observations across the entire continent, analyzing data recorded at the 190 sites equipped with portable broadband seismic recorders for a time span of recording of 6 months in average, and did not find any clear pattern of anisotropy at the continental scale. At a more regional scale however, anisotropy frozen in the lithosphere can be highlighted along the southeastern coast of the continent, in the Kimberley region (northwest of the continent), and a possible curvilinear trend subparallel to the structural trends of some aspects of the TL, as defined by various authors, is highlighted. On the other hand, the complex evolution of the continent may have produced a rather complex lithosphere-asthenosphere boundary, as seen in surface wave tomography [*Debayle and Kennett*, 2000b; *Fishwick et al.*, 2005; *Kennett et al.*, 2004a, 2004b; *Simons et al.*, 1999]. The mantle flow underneath the continent could therefore be far more complex than simply related to APM, and deviation around the various cratonic keels could be envisioned. Taking into account 2 years of data recording at the stations deployed within the framework of the TASMAL experiment, the pattern of anisotropy drastically changes in eastern Australia, highlighting evidence of isotropy underneath numerous seismological stations [*Heintz and Kennett*, 2006].

2.2. Source Side

[14] The location of the Australian continent with respect to the surrounding subduction zones represents a very suitable place to record direct S waves. The Australian plate is surrounded by subduction zones to the north (Java, Sumatra, Philippines) and east (New Hebrides, Fiji, Tonga, Kermadec, see Figure 1). These regions are sources of a very high seismic activity down to at least 650 km depth.

[15] In the Fiji-Tonga-Kermadec trenches the Pacific plate is subducted westward underneath the Australian plate, whereas at the New Hebrides trench the Australian plate subducts northeast beneath the Pacific plate. The Fiji-Tonga subduction zone appears to be rather complex: the Wadati-Benioff plane is very steep (~60°) from 32°S to 20°S latitude, whereas further north, its dip is gentle. Toward the north, events occur mainly down to 200 km depth, with only a few events located deeper.

[16] The Fiji-Tonga subduction zone has been extensively studied, by means of tomography [e.g., *Gorbatov and Kennett*, 2003; *van der Hilst*, 1995; *Widiyantoro et al.*, 1999] as well as shear wave splitting investigations [e.g., *Chen and Brudzinski*, 2003; *Fischer and Wiens*, 1996]. Using traveltime P wave tomography, *van der Hilst* [1995] highlighted a complex morphology of the subducting Pacific plate, showing north-south variations. In the northern part (between 15°S and 25°S latitude), the slab deflects in the transition zone (400–700 km depth) before plunging with a steep angle into the lower mantle. Further south, the penetration into the lower mantle is straight.

[17] Joint tomographic inversions of P and S wave data focused on northwest Pacific island arcs [*Gorbatov and Kennett*, 2003; *Widiyantoro et al.*, 1999] confirmed penetration into the lower mantle for the Pacific plate subducting below Fiji-Tonga, as well as flattening above the 660 km discontinuity.

[18] *Fischer and Wiens* [1996] studied the depth distribution of mantle anisotropy beneath Tonga and concluded that the good consistency observed between direct S waves and core refracted shear waves splitting parameters is strong evidence that splitting due to lower mantle anisotropy beneath Tonga is negligible. The similarity of SKS and local S splitting is most plausibly explained by models in which the bulk of the lower mantle is virtually isotropic.

[19] *Chen and Brudzinski* [2003] on the other hand demonstrated an unequivocal case of anisotropy in the transition zone beneath Fiji-Tonga from horizontally polarized shear waves arriving up to 3 s earlier than vertically polarized shear waves, at stations located in the back arc and fore arc of the trench.

[20] The overall morphology of the subducting Pacific plate beneath Fiji-Tonga seems well constrained, highlighted by a steep dip into the upper mantle followed by a flattening in the transition zone, whereas the plate penetrates into the lower mantle several hundred kilometers further west without any kink. The characterization in terms of anisotropy in this region is however less well constrained.

[21] Toward the northwest of the Australian continent, the Australian plate subducts under Eurasia and the southwest Philippine plate plunges toward the west underneath the Eurasian plate. Tomographic studies [e.g., *Gorbatov and Kennett*, 2003] tracked the slab down to 1500 km depth. The subduction of the Indo-Australian plate under Eurasia occurs along the Sunda arc and is rather complex.

[22] Several tomographic studies led in this region [*Puspito et al.*, 1993; *Widiyantoro and van der Hilst*, 1996, 1997], mainly based on tomographic inversion of traveltime residuals of direct P waves, highlight a variation in the morphology of the subducting slab; beneath Java, the steeply dipping (~60°) lithospheric slab descends into the lower mantle. A reduced amplitude of the wave speed

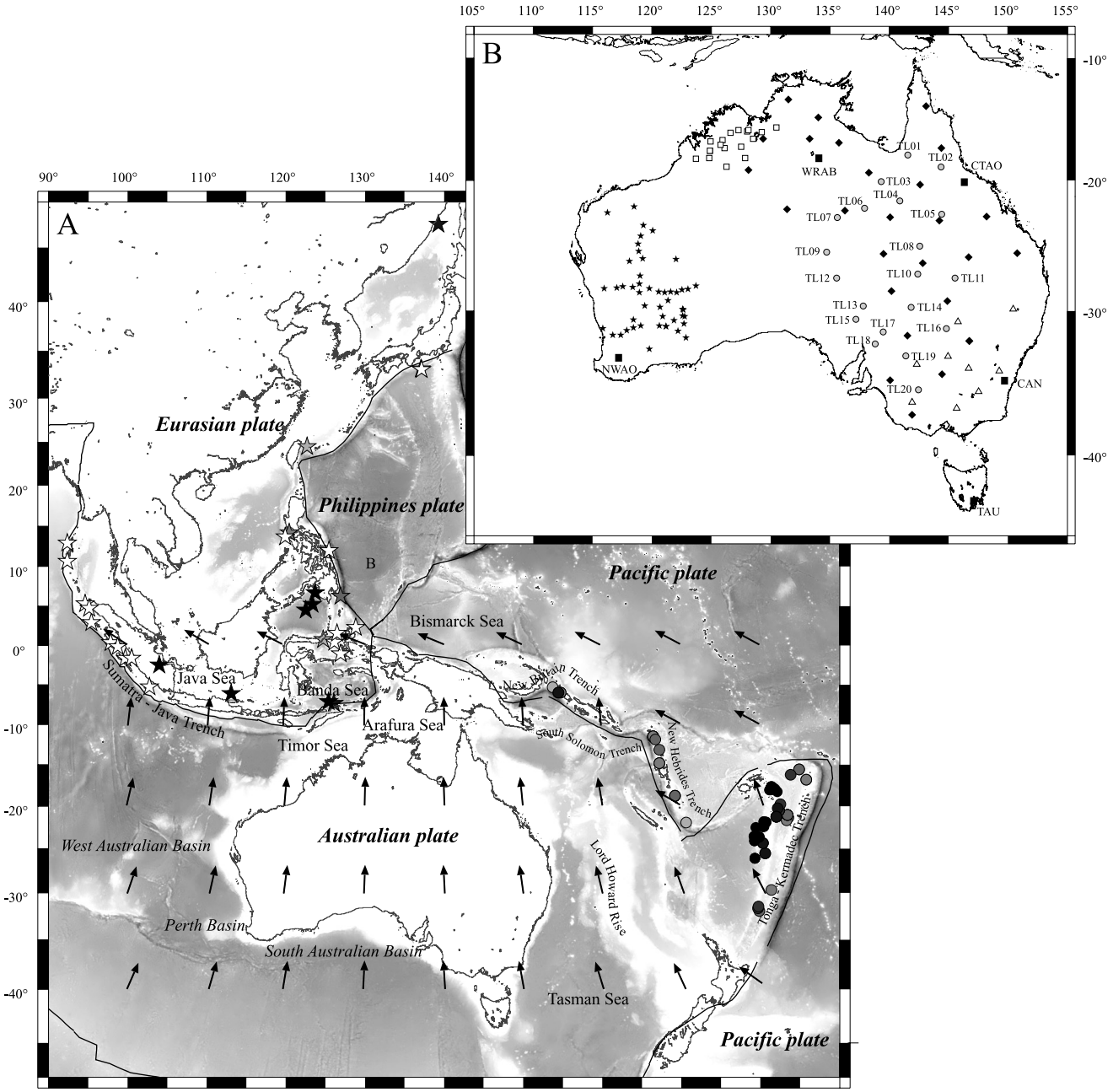

Figure 1. (a) Geodynamical context of the region of interest. Names of the plates and subduction zones surrounding the Australian plate to the north and east are shown. The black line represents the plate boundaries. The circles and stars represent the epicenters of the events studied. They are color coded with respect to depth: white standing for the shallowest and black for the deepest. The arrows represent the orientation of the Australian APM as defined by HS3-NUVEL-1A model [*Gripp and Gordon*, 2002]. The arrows all have the same length; the plate velocity is not taken into account in this representation. (b) Location of the various temporary deployments considered in the present study are plotted on the Australian continent: TASMAL (grey circles), SKIPPY (solid diamonds), QUOLL (open triangles), KIMBA (open squares), and WACRATON (solid stars). For comparison sake with other studies, the permanent stations are plotted as solid squares.

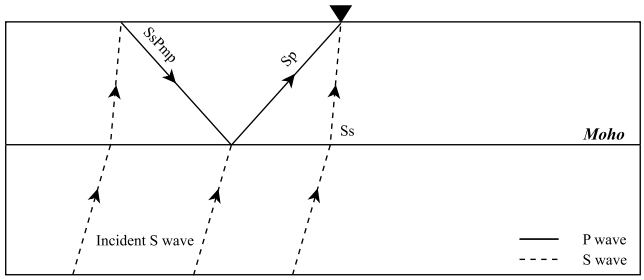

Figure 2. Ray paths of shear coupled P waves in the crust. Sp results from a S-to-P conversion at the Moho beneath the station. SsPmp is a S wave converted to a P wave at the free surface and then reflected up to the site at the Moho.

anomaly in the seismic gap, between 350 and 500 km depth, may suggest a thinning of the slab, which then appears to be deflected in the upper lower mantle. This kink in the slab gradually decreases toward the west. Under Sumatra, the slab is almost vertical in the lower mantle, with an indication that the deep part of the slab is detached from the seismogenic slab in the transition zone.

3. Data and Method

3.1. Acquisition

[23] Since 1992, the Research School of Earth Sciences, Australian National University, has been involved in a very comprehensive deployment of seismological stations at the scale of the Australian continent. This provides coverage of a continent that has not been previously achieved anywhere else (Figure 1b). The successive deployments include: SKIPPY, an itinerant deployment of 10 broadband recorders for a 6 month period resulting in the coverage of the continent within 3 years (1993–1996) [*van der Hilst et al.*, 1994]; KIMBA, a seismic deployment in the Kimberley region (NW of the continent) between 1997 and 1998; QUOLL, a set of 10 seismic recorders located in SE Australia in 1999; and WACRATON (2000–2001 then 2002–2003), consisting of three lines of instruments covering roughly N-S and E-W transects in western Australia. The most recent deployment undertaken is the TASMAL experiment; this consists of 20 broadband seismometers deployed for a 2-year period (2003–2005) in eastern Australia, spanning from northern Queensland to southern Victoria. The aim of the TASMAL project is to record a reliable data set on both sides of the hypothetical and controversial TL, in order to produce an accurate seismic image of the lithosphere in its vicinity using various seismological tools. As seismic anisotropy helps mapping potential evidence of flow inside the Earth, its study is of particular interest along a boundary or suture between two basements of various ages that underwent a collisional event, in order to differentiate between APM related and frozen-in anisotropy theories.

3.2. Selection Criteria

[24] The events occurring in the subduction zones surrounding Australia were selected with respect to epicentral distance (24–80°), magnitude (>5.5 Mb) and a good signal-to-noise ratio (visual inspection), in order to have distinct and energetic direct S waves. All depths have been considered, but in the following, events are classified in two categories: ''deep'' for those events occurring below 410 km depth, and ''intermediate and shallow'' for those occurring above 409 km depth. Events are also classified by epicentral locations: events mainly occurring in the Java-Sumatra region are in the back-azimuthal range 280–360°, whereas those occurring in the Fiji-Tonga subduction zone are in the back-azimuthal range 60–120°.

3.3. Method

[25] Shear wave splitting measurements were performed using the *Silver and Chan* [1991] algorithm in the case where the initial polarization direction of the incoming wave is assumed to be unknown. This method consists of finding the splitting parameters that minimize the smaller eigenvalue of the covariance matrix of corrected particle motion, hence revealing the most linear particle motion. The errors in the results are estimated by applying a statistical *F* test and using the extent of the 95% confidence interval. This method considers homogeneous seismic anisotropy in a single horizontal layer and is only applicable to shear waves arriving at the station with nearly vertical incidence. For direct S waves showing a larger angle of incidence, the near-receiver reverberations and conversions may have enough amplitude to interfere with the S wave coda, and thus one has to be cautious when analyzing the traces and check whether or not the signal is contaminated by shear-coupled P waves.

[26] Data are mostly not filtered, but when applied, a four-pole Butterworth band pass with corner frequencies at 0.03 Hz and 0.35 or 0.55 Hz was used. The data are windowed around the phase of interest based on the predicted traveltimes from the iasp91 Earth model [*Kennett and Engdahl*, 1991]. Potential contamination of shear coupled P waves, inferred from the existence of a phase with nonnegligible amplitude a few seconds after the arrival of the direct S wave, has been carefully checked. These shear coupled P waves are generated from the incidence of teleseismic or deep regional SV waves at major interfaces in the crust and at the free surface: these long-period P disturbances are excited by conversion at the Moho and reverberate in the crust. A schematic of the ray paths of some of these arrivals is presented in Figure 2 for Sp and SsPmp phases. *Wookey and Kendall* [2004] performed a wave decomposition in their data set recorded at the Australian permanent stations and showed that significant shear-coupled P wave energy in the analysis window would significantly degrade the estimate of confidence in the shear splitting results, but the intrinsic values would be little affected; the results from both their studies however showed a distinct decrease in the value of dt, from 0.7–7.1 s [*Wookey et al.*, 2002] to 0.7–6.2 s [*Wookey and Kendall*, 2004].

[27] Figures 3 and 4 show examples of the influence of filtering and data windowing. In the first case (Figure 3), I demonstrate the influence of shear coupled P waves in the measurement window, whereas the influence of a PcS phase is observed in the second case (Figure 4). A measurement performed on one event recorded at the permanent WRAB station, previously resulted in a delay of 3.95 s and an orientation of the polarization plane of the fast S wave trending N3°W [*Wookey et al.*, 2002]. The raw data itself might look ambiguous (Figure 3) due to the two peaks of energy observed on the E-W component of the seismogram,

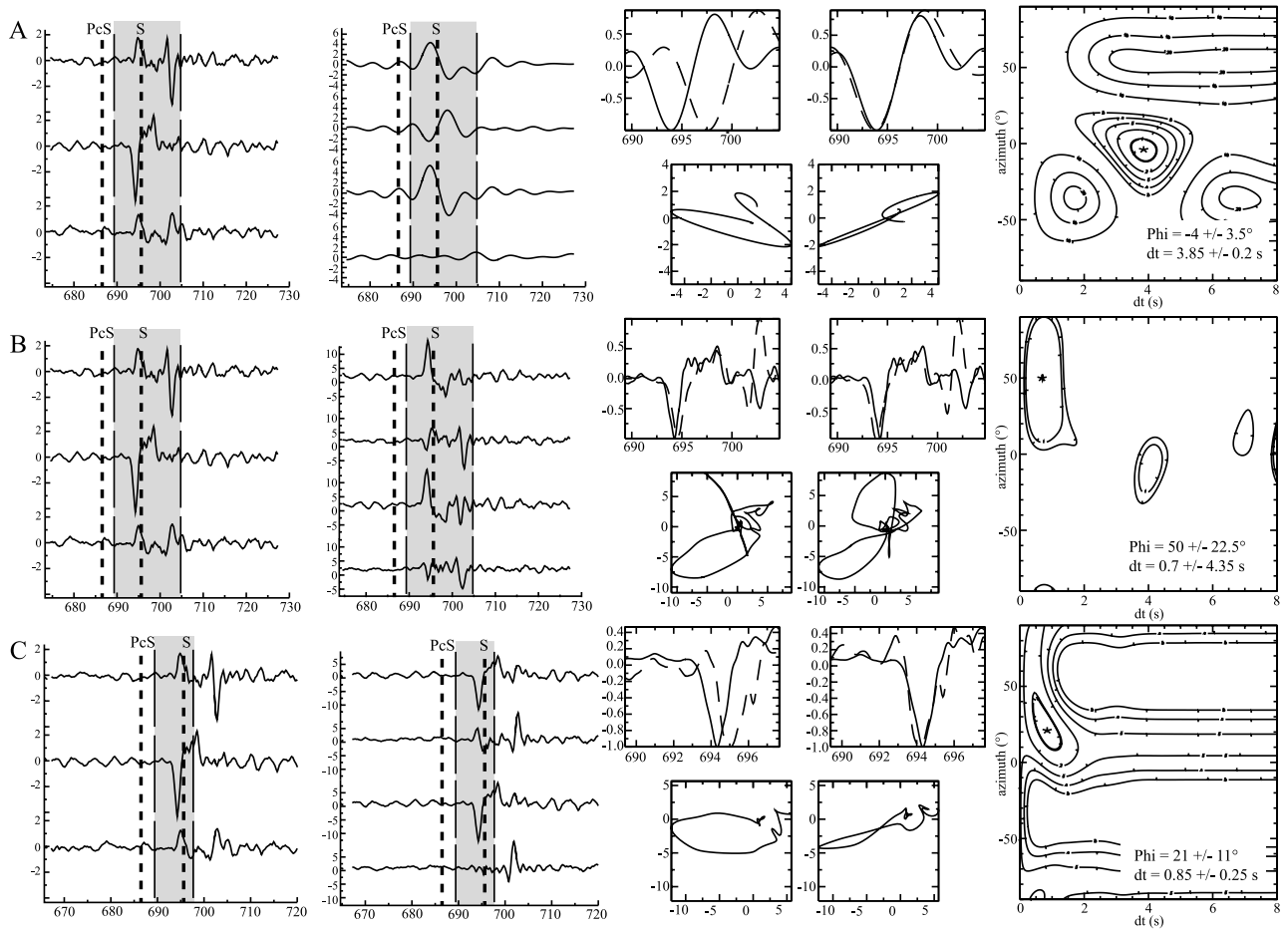

Figure 3. Effects of the variations of filtering and data windowing on one event (latitude −31.16°, longitude 179.62°, depth 449 km) recorded at the permanent station WRAB. The measurements are performed following *Silver and Chan*'s [1991] algorithm. For each measurement (Figures 3a, 3b, or 3c), from left to right, the first panel represents the event recorded in the geographical referential (E-W, N-S and vertical). The top two traces in the second panel correspond to the event rotated into the radial and transverse components before correction of anisotropy, whereas the bottom two traces represent the same components after anisotropy removal. The grey box on these first two plots represents the measurement window, and the dashed lines represent the theoretical arrival time of the PcS and S phases according to the IASP91 model [*Kennett and Engdahl*, 1991]. The third panel shows the waveform of the fast (dashed line) and slow S waves (left) before and (right) after correction of the anisotropy, respectively associated with the particle motion. The fourth panel represents the contour plot of energy and the double contour outlines the 95% confidence interval. (a) Measurement window considered to be relatively large, including the direct S wave and the following peak of energy. The data are highly filtered using a Butterworth band-pass filter between 0.02 and 0.15 Hz. Once filtered, the second peak of energy disappears. The two waveforms before and after anisotropy removal are similar, and the particle motion becomes linear after anisotropy removal. The solution is well constrained highlighting phi of 4 ± 3.5° and dt of 3.85 ± 0.2 s in good agreement with *Wookey et al.* [2002] result. (b) Same measurement window as in Figure 3a, but with unfiltered data. Note the complexity of the waveform and the randomness of the particle motion. The solution radically differs from the previous one and is not well constrained at all (phi = 50 ± 22.5° and dt = 0.70 ± 4.35 s). (c) Measurement window shortened to only include the direct S wave. The data are not filtered. The two waveforms are similar, shifted from dt before the correction of anisotropy and well superimposed after. The particle motion changes from elliptical to linear with the anisotropy removal, and the solution is well constrained (phi = 21 ± 11° and dt = 0.85 ± 0.25 s). This is the value I would keep.

respectively the direct S wave and a potentially shear coupled P wave. Performing the measurement on a large window including both peaks without filtering leads to phi = 50 ± 22.5° and dt = 0.7 ± 4.35 s, i.e., a "poor" measurement regarding the associated errors (see below for the classification of the results). Performing the measurement on the same data using a Butterworth band pass with corner frequencies at 0.02 and 0.15 Hz, gives phi = −4 ± 3.5° and dt = 3.85 ± 0.2 s,

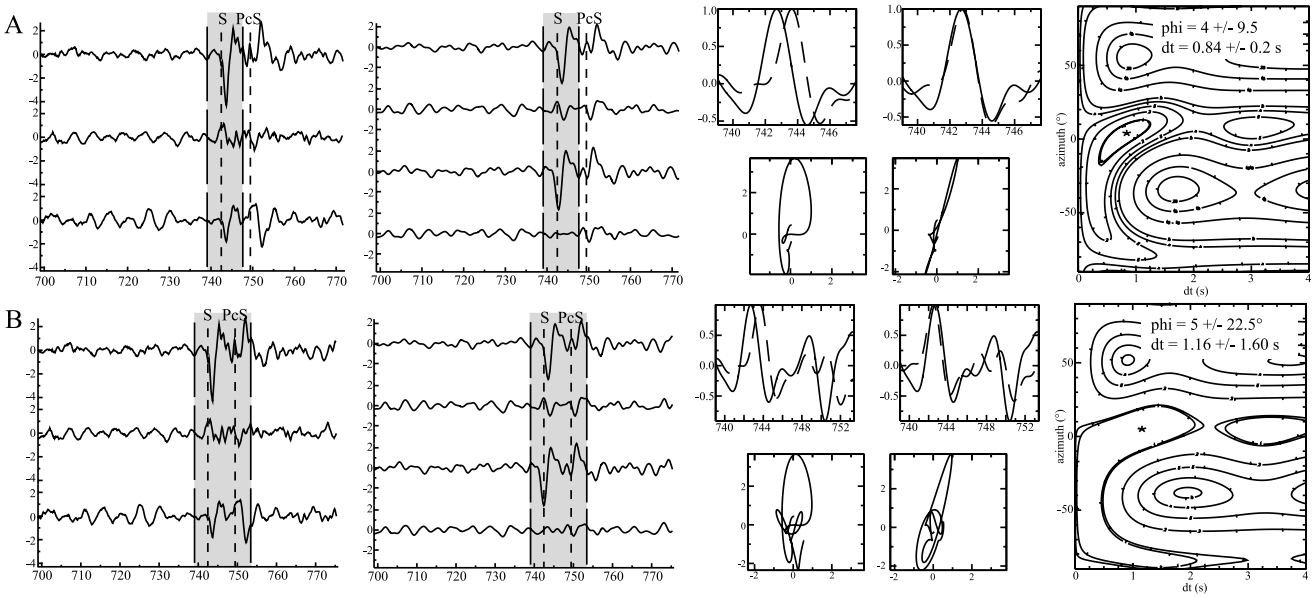

Figure 4. Influence on the splitting measurements of the presence of a PcS phase in the measurement window for one event (event 2003.284) recorded at station TL06. The description of the various diagrams is the same as for Figure 3. (a) Measurement window restricted to the direct S wave and the data filtered between 0.03 and 0.55 Hz. The measurement is good, highlighting a nice superimposition of the two waveforms after correction of the anisotropy together with a linear particle motion. The errors associated with the measurement are small (phi = 4 ± 9.5° and dt = 0.84 ± 0.20 s). (b) Measurement window now including the PcS phase. To compare with the previous measurement, the data are filtered using a Butterworth band-pass filter between 0.03 and 0.55 Hz. The waveforms of the fast and slow S waves are more complex, and the superimposition is not as good as in Figure 4a. The associated particle motion is also more complex. It results in a similar solution, but with high associated errors similar to what could be expected in the case of an undetermined solution (phi = 5 ± 22.5° and dt = 1.16 ± 1.60 s).

similar to that of *Wookey et al.* [2002]. On the other hand, if the window includes only the direct S wave arrival, and no filter is applied, I obtain phi = 21 ± 11° and dt = 0.85 ± 0.25 s.

[28] I show in Figures 4a and 4b an example of splitting measurements performed for one event recorded at station TL06, with the measurement window strictly restricted to the S wave in the first case, and extended to include the PcS phase (P-to-S converted reflection from the CMB) in the second case. When the window is extended to include the PcS phase, the intrinsic splitting parameters are not fundamentally changed (phi = 5° and dt = 1.16 s in case b versus phi = 4° and dt = 0.84 s in case a), but the errors rise to respectively ±22.5° and ±1.60 s, compared to ±9.5° and ±0.2 s in case a. This suggests that potential contamination due to PcS waves could significantly affect the estimate of confidence in the shear wave splitting results, but not the intrinsic values of phi and dt.

[29] Results appear to be therefore highly variable, and in this study, care has been taken with respect to the inclusion of shear coupled P or PcS phases in the measurement window. Several filters have been applied on the data, and only those showing no variation in the results (up to 15° for phi and up to 0.3 s for dt) have been considered as reliable and kept. I therefore have good confidence in the validity of the results shown in the present study.

3.4. Classification of the Results

[30] All the splitting results produced in the present study are listed in Tables 1 and 2, as a function of the source region and the depth location of the events. The classification of the results (good, fair and poor) is based on four quality criteria: (1) the quality of the signal-to-noise ratio, (2) the ellipticity of the particle motion in the horizontal plane when anisotropy is present, (3) its linearization by anisotropy removal, and (4) the waveform coherence between the fast and slow split shear waves. Measurements satisfying all four criteria well are rated as ''good'' and those for which only three criteria are satisfied are rated as ''fair.'' Poor measurements only fulfill two criteria and have been discarded. Only good and fair measurements have been kept and the selection has been rather critical, giving therefore good confidence in the data set obtained. A particular category concerns the null measurements. A ''null'' does not show any energy on the transverse component associated with the arrival of the core phase of interest on the radial component; this may be due either to an absence of anisotropy or to an initial polarization of the incoming wave parallel or orthogonal to the fast anisotropic direction. Null measurements of high quality have also been included in the tables of results.

4. Results

4.1. Back-Azimuthal Range 60–120°: Fiji-Tonga

[31] A total of 125 measurements, classified either good (51), fair (63) or null (11), has been considered, resulting from 67 events occurring in the Fiji-Tonga subduction zone.

Table 1. Anisotropic Parameters With Associated Errors Resulting From Measurements Performed on Events Occurring in the Back-Azimuthal Range 60–120° (Fiji-Tonga Subduction Zone) and Recorded at Various Temporary Deployments Across the Australian Continent[a]

Events	Station	Elat	Elon	Dist	Baz	Depth	phi	err_{phi}	pol	dt	err_{dt}	Quality
Deep Events Back-Azimuthal Range 60–120°												
TASMAL												
2003.240	TL06	−21.98	−179.58	39.2	97.9	602	12	12.5	85.9	0.8	0.12	fair
2003.284	TL03	−17.9	−178.57	39.7	94	597	84	13	10	1.2	0.4	fair
2003.284	TL06	−17.9	−178.57	41	92	597	4	9.5	88	0.84	0.2	good
2003.284	TL15	−17.9	−178.57	42	82.8	597	0					null
2003.288	TL06	−17.82	−178.7	40.9	91.8	582	0	7	91.8	0.76	0.08	fair
2003.288	TL07	−17.82	−178.7	42.9	91.8	582	−2	10	93.8	0.4	0.08	good
2003.288	TL10	−17.82	−178.7	37	83.4	582	−39	10.5	122.4	0.64	0.08	good
2003.288	TL12	−17.82	−178.7	43.1	86.9	582	20					null
2003.296	TL02	−23.7	179.8	33.2	104.5	503	35	8.5	69.5	2.92	0.24	fair
2003.296	TL06	−23.7	179.8	38.5	100.5	503	3	5	97.5	0.84	0.16	fair
2003.296	TL08	−23.7	179.8	33.8	95.4	503	−13	8	108.4	0.8	0.08	fair
2003.324	TL06	−24.37	−179.71	38.8	101.6	480	7	4	94.6	0.8	0.8	good
2003.324	TL10	−24.37	−179.71	34.1	93.6	480	−9	17.5	102.6	0.4	0.12	good
2003.339	TL02	−26.12	179.27	32.9	109	509	23	11	86	0.36	0.08	fair
2003.339	TL03	−26.12	179.27	37	106.9	509	5	14	101.9	1.4	0.2	fair
2003.339	TL06	−26.12	179.27	37.8	104.3	509	12	5	92.3	0.8	0.12	good
2004.108	TL10	−23.66	179.87	33.9	92.2	543	0	8	92.2	0.56	0.08	good
2004.183	TL05	−25.54	−179.38	33	102.3	405	65	10	37.3	1	0.16	fair
2004.183	TL06	−25.54	−179.38	39	103.5	405	21	3	82.5	1.96	0.08	good
2004.197	TL06	−17.64	−178.62	41	91.6	560	10	14.5	81.6	0.8	0.24	good
2004.197	TL12	−17.81	−178.7	43.1	86.9	560	18	11	68.9	0.52	0.16	good
2004.322	TL05	−20.07	−178.71	34.3	92.6	622	27	12	65.6	0.56	0.08	fair
2004.352	TL07	−21.9	−179.3	41.5	97.6	593	−7	8	104.6	0.56	0.12	good
2004.352	TL17	−21.9	−179.3	37.8	85.4	593	24	3.5	61.4	0.72	0.12	fair
2004.354	TL14	−18.1	−178.85	37.5	80.9	563	13	3.5	67.9	1.2	0.16	fair
2004.354	TL17	−18.1	−178.85	39.8	80.3	563	32	8	48.3	0.48	0.04	good
2005.058	TL14	−17.72	−178.59	37.9	80.5	555	−45	4.5	125.5	1.52	0.08	fair
2005.078	TL12	−21.89	−179.55	41	92.2	598	18	6.5	74.2	0.4	0.04	good
2005.078	TL14	−21.89	−179.55	35.4	86.3	598	24	7	62.3	0.76	0.08	good
2005.089	TL08	−22.46	−179.75	34.4	93.4	588	2	12.5	91.4	0.92	0.16	good
2005.089	TL12	−22.46	−179.75	40.6	92.9	588	2	7.5	90.9	0.48	0.04	good
QUOLL												
1999.099	QR09	−26.354	178.221	29.4	78.3	621	−40	5.5	118.3	0.88	0.08	good
1999.177	QR07	−17.956	−178.19	38.6	75.7	590	46	10.5	29.7	1.28	0.12	fair
1999.199	QR01	−22.546	179.412	26.8	80.9	591	71					null
1999.202	QR01	−18.289	−177.91	30.9	75.2	561	−3	6.5	78.2	0.8	0.12	fair
SKIPPY												
1993.196	SA05	−23.604	179.157	32	97.8	548	80	7	17.8	0.76	0.08	good
1993.196	SA03	−23.604	179.157	33.9	102.3	548	27	13	75.3	0.44	0.08	good
1993.196	SA04	−23.604	179.157	35.8	98.9	548	6					null
1993.233	SA01	−21.278	−178.02	37.6	106.8	427	−3	6.5	109.8	1.24	0.2	fair
1993.233	SA04	−21.278	−178.02	38.7	95.8	427	−13	10.5	108.8	1.12	0.28	fair
1993.233	SA05	−21.278	−178.02	34.9	94.3	427	90	2	4.3	1.12	0.08	fair
1993.233	SA07	−21.278	−178.02	32.5	89.1	427	−19	12	108.1	0.32	0.08	fair
1993.323	SB01	−22.427	−179.57	37.3	93.7	591	−19	7.5	112.7	0.92	0.08	fair
1993.323	SB02	−22.427	−179.57	34.3	91.5	591	−81	9.5	172.5	0.52	0.08	fair
1993.344	SB02	−22.18	−179.58	34.4	91	605	−62	17	153	0.56	0.16	good
1993.344	SB03	−22.18	−179.58	36.7	89.3	605	31	9	58.3	1.12	0.08	fair
1994.047	SB08	−26.271	178.273	32.6	80.7	606	34	5	46.7	1.32	0.12	fair
1994.068	SB08	−18.039	−178.41	39.7	71.9	563	86	13	−14.1	1.16	0.24	fair
1994.090	SB09	−22.057	−179.53	31.5	79.6	580	5	8	74.6	1.6	0.36	fair
1994.110	ZB12	−17.8	−178.4	31	70.3	543	21	5	49.3	1.52	0.2	fair
1994.273	SC03	−21.217	−179.29	48.7	103.8	643	53	14	50.8	0.32	0.08	fair
1994.273	SC08	−21.217	−179.29	45.7	98.4	643	11	3.5	87.4	0.72	0.08	good
KIMBA												
1997.238	KA02	−25.511	178.331	47.8	110	610	33	11	77	1.32	0.08	fair
1997.250	KA02	−6.017	154.458	27.8	72	421	−75	8.5	147	1.16	0.28	fair
WACRATON												
2000.246	WR02	−20.07	−179.13	56.2	98.8	687	39	17.5	59.8	0.32	0.08	fair
2000.246	WR04	−20.07	−179.13	54.2	96.6	687	−5	9	101.6	0.48	0.12	good
2000.353	WR02	−21.18	−179.12	55.9	100.1	628	9	8.5	91.1	0.56	0.08	good
2000.353	WR04	−21.18	−179.12	53.8	97.9	628	−1	10.5	98.9	0.48	0.08	good
2000.353	WR07	−21.18	−179.12	53.1	96.1	628	−11	9	107.1	1	0.2	good
2000.353	WR08	−21.18	−179.12	56.4	96.2	628	−15	18.5	111.2	0.28	0.16	fair

Table 1. (continued)

Events	Station	Elat	Elon	Dist	Baz	Depth	phi	err_{phi}	pol	dt	err_{dt}	Quality
2000.353	WT02	−21.178	−179.12	57.8	96.3	628	−18	2.5	114.3	1.32	0.12	good
2000.353	WT05	−21.178	−179.12	56.3	95.8	628	−2	7.5	97.8	0.68	0.08	good
2000.353	WT06	−21.178	−179.12	55.9	95.7	628	−10	−19	105.7	0.36	0.16	fair
2000.353	WT08	−21.178	−179.12	54.5	95	628	27	20.5	68	0.6	0.16	fair
2000.353	WT10	−21.178	−179.12	52.9	94.6	628	31	10.5	63.6	0.52	0.12	good
2002.344	WP02	−24.14	179.24	55.1	100.9	530	1					null
2002.344	WP03	−24.14	179.24	54.3	100.6	530	−5					null
2003.139	WP16	−18.04	−178.67	55.7	91.4	563	−62	7.5	153.4	1.8	0.4	fair
					Shallow and Intermediate Events Back-Azimuthal Range 60–120°							
					TASMAL							
2003.133	TL18	−17.29	167.74	30.1	66.8	33	49	5.5	17.8	0.92	0.12	good
2003.203	TL09	−15.42	166.14	31	76.9	33	78	11.5	−1.1	0.64	0.08	fair
2003.203	TL15	−15.42	166.14	30.5	66.6	33	−87	7	153.6	1.28	0.12	good
2003.208	TL03	−21.08	−176.59	41.1	99.3	212	1	7	98.3	1.8	0.12	good
2003.208	TL15	−21.08	−176.59	42.4	88.2	212	16	6.5	72.2	0.96	0.2	good
2003.208	TL16	−21.08	−176.59	35.9	82.8	212	−11	11.5	93.8	1.4	0.4	fair
2003.242	TL03	−14.8	167.24	27.1	83.1	137	27	5.5	56.1	2.64	0.28	fair
2003.242	TL10	−14.8	167.24	26.2	66.5	137	−38	11	104.5	0.64	0.2	fair
2003.242	TL18	−14.8	167.24	31.2	62.3	137	4	2	58.3	3.08	0.08	fair
2003.350	TL13	−18.91	−177.34	42	85.6	381	27					null
2004.011	TL03	−16.24	−176.18	42.3	92.2	366	11	11	81.2	0.96	0.32	good
2004.025	TL07	−16.83	−174.2	47.4	92.1	129	31	11	61.1	1.2	0.2	fair
2004.025	TL18	−16.83	−174.2	45	81.3	129	62	12	19.3	1	0.16	fair
2004.032	TL06	−31.66	179.7	38.2	113.3	354	14	15	99.3	0.92	0.24	fair
2004.051	TL03	−11.61	166.45	27.3	76	84	2	6.5	74	1.2	0.12	good
2004.051	TL06	−11.61	166.45	29.2	73.4	84	70					null
2004.072	TL06	−15.58	−175.1	44.8	90	271	18	13	72	1.84	0.36	fair
2004.072	TL10	−15.58	−175.1	41	82.3	271	20	18.5	62.3	1.16	0.28	fair
2004.100	TL06	−13.18	167.21	29.2	77	229	77		0			null
2004.100	TL17	−13.17	167.2	31.3	60.3	228	30	3.5	30.3	1.72	0.28	fair
2004.128	TL18	−21.99	170.28	29.7	77.3	14	14	4	63.3	2.2	0.2	fair
2004.128	TL15	−21.99	170.28	30.8	81.6	14	14					null
2004.225	TL04	−11.91	166.72	26.5	72.6	205	12	6.5	60.6	1.04	0.2	fair
2005.101	TL12	−21.98	170.61	32.2	87.8	68	−3	4	90.8	1.28	0.12	very good
					QUOLL							
1999.103	QR08	−21.422	−176.46	34.4	75.1	164	88	7	−12.9	2.8	0.72	fair
					SKIPPY							
1993.190	SA06	−19.782	−177.49	32	91	398	6	4.5	85	1.8	0.16	fair
1994.042	SB02	−18.773	169.169	25.4	77.8	206	63	10	14.8	2.52	0.24	fair
1994.042	SB03	−18.773	169.169	28.2	76.1	206	25	8	51.1	1.44	0.12	good
1994.042	SB08	−18.773	169.169	30.2	59.5	206	5	4.5	54.5	2.72	0.2	fair
1994.234	SC03	−11.509	166.452	36.3	86.9	142	19	8.5	67.9	0.68	0.12	good
1994.234	SC04	−11.509	166.452	32.5	85.4	142	−44	17	129.4	0.36	0.16	good
1994.234	SC06	−11.509	166.452	37.7	84.1	142	18	6.5	66.1	0.88	0.08	good
1994.234	SC10	−11.509	166.452	34.1	72.6	142	−2	5.5	74.6	0.84	0.12	good
1994.285	SC06	−6.936	155.781	29.5	69.4	49	17	6	52.4	1.12	0.12	good
1994.361	YB05	−31.965	179.86	27.6	80.8	212	−39	6.5	119.8	1.2	0.12	good
					KIMBA							
1997.238	KA02	−25.511	178.331	47.8	110	610	33	11	77	1.32	0.08	fair
1997.250	KA02	−6.017	154.458	27.8	72	421	−75	8.5	147	1.16	0.28	fair
					WACRATON							
2000.228	WS06	−31.511	179.725	53.5	112.1	357	69	18	43.1	1	0.4	fair
2000.323	WT02	−5.228	151.771	42.2	58.6	33	−29					null
2001.019	WR02	−11.66	166.38	45.7	82.9	50	23	16.5	59.9	0.68	0.16	fair
2001.019	WR04	−11.66	166.38	44.2	79.6	50	82	4	−2.4	1.92	0.28	fair
2001.019	WR07	−11.66	166.38	44.2	76.9	50	−18	4	94.9	1.92	0.12	fair
2001.019	WR08	−11.66	166.38	48.2	77.6	50	47	2	30.6	1.72	0.12	good
2001.019	WR09	−11.66	166.38	44.9	73.2	50	23	6	50.2	1.12	0.08	good
2001.146	WR08	−20.29	−177.84	57.9	95.8	406	−67	15	162.8	0.72	0.16	good
2001.152	WR08	−7.2	154.92	41.5	63.3	33	−30	4.5	93.3	1.84	0.24	fair
2001.154	WR08	−29.67	−178.63	53.8	106.1	178	16	7	90.1	0.92	0.12	good
2001.185	WR09	−21.73	−176.71	54.3	95	184	−51	3.5	146	2	0.32	good
2003.004	WP03	−20.57	−177.66	58.2	97.7	378	−74	4	171.7	1.36	0.24	good
2003.004	WP04	−20.57	−177.66	57.8	97.7	378	−81	10	178.7	1.88	0.44	fair
2003.004	WP06	−20.57	−177.66	57.7	97.3	378	−79	3.5	176.3	1.44	0.12	good
2003.004	WP11	−20.57	−177.66	57.2	96.5	378	−80	4.5	176.5	1.68	0.32	fair
2003.010	WP02	−5.31	153.7	41.3	63.2	71	−56	8	119.2	1.88	0.36	fair
2003.041	WP02	−6.01	149.79	37.8	60.3	33	−55	14	115.3	1.92	0.36	fair

Table 1. (continued)

Events	Station	Elat	Elon	Dist	Baz	Depth	phi	err_{phi}	pol	dt	err_{dt}	Quality
2003.163	WP15	−5.99	154.76	40.3	58.5	186	−13	5.5	71.5	0.56	0.08	very good
2003.163	WP17	−5.99	154.76	39.1	57.1	186	−18	16	75.1	0.56	0.16	very good
2003.208	WP15	−21.08	−176.59	56.2	95.7	212	5	18.5	90.7	0.88	0.32	fair

[a]The values correspond to events, Julian date of the event; station, station name; Elat, event latitude; Elon, event longitude; Dist, epicentral distance; Baz, back azimuth; depth, event depth; phi; err_{phi}, error on phi; pol, polarization of the fast shear wave as the back azimuth minus the measured phi; dt; err_{dt}, error on dt; and quality of the measurement.

Table 2. Anisotropic Parameters With Associated Errors Resulting From Measurements Performed on Events Occurring in the Back-Azimuthal Range 280–360° (Mainly Java-Sumatra Subduction Zone) and Recorded at Various Temporary Deployments Across the Australian Continent[a]

Events	Station	Elat	Elon	Dist	Baz	Depth	phi	err_{phi}	pol	dt	err_{dt}	Quality
Deep Events Back-Azimuthal Range 280–360°												
TASMAL												
2003.146	TL09	6.76	123.71	34	340.1	565	1	14.5	339.1	0.28	0.08	fair
2003.146	TL13	6.76	123.71	38.8	337.1	565	86	4	251.1	0.96	0.16	fair
2003.146	TL16	6.76	123.71	43	328.3	565	−39					null
2003.146	TL19	6.76	123.71	43.3	333.8	565	89	8	244.8	0.48	0.12	good
2003.182	TL01	4.53	122.51	29.3	318.1	635	18	9	300.1	0.32	0.04	good
2003.182	TL02	4.53	122.51	31.8	315	635	43	10	272	1	0.2	good
2003.182	TL03	4.53	122.51	29.6	324.1	635	39	7	285.1	0.68	0.04	good
2003.182	TL04	4.53	122.51	31.7	323.1	635	5	9	318.1	0.8	0.08	fair
2003.182	TL05	4.53	122.51	34.6	318.9	635	20	10.5	298.9	0.68	0.08	good
2003.182	TL06	4.53	122.51	30.6	328.6	635	6	3.5	322.6	0.88	0.08	good
2003.182	TL18	4.53	122.51	40	334.1	635	65					null
2003.208	TL04	47.15	139.25	68.5	358.7	470	−7	9	365.7	1.28	0.12	good
2003.208	TL06	47.15	139.25	69.1	0.9	470	−29	13	29.9	2.04	0.24	fair
2003.208	TL10	47.15	139.25	74.2	357.7	470	−27	5	384.7	1.6	0.16	good
2003.208	TL11	47.15	139.25	74.7	355.5	470	−18	7.5	373.5	1.04	0.16	fair
2003.208	TL13	47.15	139.25	76.5	1	470	−41	15.5	42	0.76	0.24	good
2003.208	TL16	47.15	139.25	78.4	356.1	470	−17	15	373.1	1.08	0.24	fair
2003.240	TL18	−7.32	126.05	27.8	331.8	409	79	11.5	252.8	0.52	0.12	fair
2003.277	TL13	−7.05	125.41	25.4	330.1	532	17	11.5	313.1	0.88	0.12	fair
2004.158	TL05	−6.04	113.11	34.5	293.9	579	78	18	215.9	0.24	0.08	fair
2004.158	TL08	−6.04	113.11	34.1	299	579	−24	7.5	323	0.8	0.12	good
2004.158	TL10	−6.04	113.11	35.1	301.9	579	−66	7.5	367.9	0.4	0.08	fair
2004.158	TL12	−6.04	113.11	30.3	311	579	54	3	257	0.4	0.08	fair
2004.207	TL04	−2.43	103.89	40.7	292.9	582	14	3	278.9	1.24	0.08	fair
2004.207	TL05	−2.43	103.98	44.2	291.3	582	33	6	258.3	0.72	0.08	good
2004.207	TL14	−2.43	103.98	45.1	299.9	582	29	8	270.9	1.76	0.12	fair
2004.207	TL17	−2.43	103.98	44.4	303.7	582	13	14	290.7	0.32	0.08	fair
2004.207	TL20	−2.43	103.98	48.7	304	582	−26	6	330	0.96	0.08	fair
2004.312	TL06	47.95	144.48	70.1	4.7	474	78	14	−73.3	1	0.28	fair
2005.036	TL12	5.29	123.34	34.8	338.3	525	64	5.5	274.3	0.8	0.08	fair
2005.036	TL14	5.29	123.34	39.2	329.9	525	17	9	312.9	0.72	0.08	good
2005.036	TL16	5.29	123.34	41.9	326.8	525	49	3	277.8	1.08	0.16	good
2005.036	TL19	5.29	123.34	42.1	332.5	525	83	6.5	249.5	0.84	0.08	good
SKIPPY												
1993.277	SA03	30.599	137.671	50.9	354.4	480	42	9	312.4	0.68	0.08	good
1993.332	SB02	−5.599	110.267	37.4	298	569	−46	6.5	344	0.6	0.08	good
1994.202	SC07	42.34	132.865	61.6	355.4	471	−17	5	372.4	2.6	0.44	fair
WACRATON												
2003.017	WP01	1.95	122.68	30.6	11.3	483	−72	4	83.3	1.76	0.44	fair
2003.017	WP02	1.95	122.68	30.4	10.4	483	−78	2.5	88.4	1.32	0.12	fair
2003.017	WP04	1.95	122.68	30	7.7	483	−83	6	90.7	3.92	0.32	fair
2003.017	WP14	1.95	122.68	33.3	1.1	483	88	6	−86.9	2.28	0.56	fair
2003.146	WP15	6.76	123.71	37.8	4.2	565	64	7.5	−59.8	0.56	0.16	good
2003.146	WP16	6.76	123.71	37.8	4.3	565	−45	4	49.3	0.64	0.04	good
2003.182	WP15	4.53	122.51	35.6	2.4	635	47	8	−44.6	0.48	0.08	fair
2003.182	WP17	4.53	122.51	35.3	359.8	635	80					null
2003.208	WP17	47.15	139.25	79.2	11.5	470	−37	5.5	48.5	1.28	0.12	good
Shallow and Intermediate Events Back-Azimuthal Range 280–360°												
TASMAL												
2003.131	TL18	−0.99	126.94	33.3	337.9	30	19	12	318.9	0.8	0.12	fair
2003.131	TL20	−0.99	126.94	37.5	333.8	30	32	8	301.8	0.84	0.16	good
2003.136	TL13	33.17	137.07	62.6	359.2	384	−5					null
2003.146	TL15	2.35	128.85	33.9	344.9	31	81	6.5	263.9	1.48	0.12	good
2003.146	TL18	2.35	128.85	36	342.8	31	87	7	255.8	1.08	0.12	fair

Table 2. (continued)

Events	Station	Elat	Elon	Dist	Baz	Depth	phi	err_{phi}	pol	dt	err_{dt}	Quality
2003.282	TL02	13.76	119.94	40.5	321.6	33	38	9.5	283.6	1.24	0.32	fair
2003.282	TL15	13.76	119.94	47.3	336.9	33	13	7	323.9	1	0.16	good
2003.291	TL04	0.44	126.1	26.3	324.7	33	4	13.5	320.7	2.24	0.44	fair
2003.316	TL04	1.59	126.48	27.1	326.7	33	32	6	294.7	1.08	0.16	fair
2003.316	TL04	33.17	137.07	54.7	356	384	−77	1.5	433	1.56	0.12	fair
2003.316	TL06	33.17	137.07	55.1	359.1	384	−85	4	444.1	1.04	0.24	fair
2003.322	TL04	12.02	125.42	36.8	334	35	11	10.5	323	0.68	0.12	fair
2003.322	TL12	12.02	125.42	40.6	344.6	35	58	10.5	286.6	0.84	0.12	fair
2004.029	TL02	6.29	126.94	30.4	323.8	209	−35	15	358.8	0.64	0.16	fair
2004.053	TL10	−1.56	100.49	47.7	295.3	42	−29	10	324.3	0.72	0.08	fair
2004.107	TL10	−5.2	102.73	43.8	293	43	55	9.5	238	1.12	0.24	fair
2004.132	TL03	0.41	97.82	45.5	291.6	21	−35	7	326.6	0.72	0.16	good
2004.132	TL05	0.41	97.82	50.9	290.4	21	47	9.5	243.4	0.72	0.2	good
2004.132	TL06	0.41	97.82	45.1	294.6	21	38					null
2004.132	TL07	0.41	97.82	43.5	297	21	40					null
2004.132	TL08	0.41	97.82	50.2	293.5	21	−27	9	320.5	0.72	0.16	good
2004.132	TL10	0.41	97.82	51	295.3	21	−56					null
2004.132	TL11	0.41	97.82	53.7	293.1	21	−55					null
2004.132	TL18	0.41	97.82	50.7	301.9	21	39	3	262.9	1.88	0.2	good
2004.182	TL02	0.8	124.73	27.6	313.1	90	43	6.5	270.1	0.96	0.12	fair
2004.182	TL03	0.8	124.73	25.3	323.6	90	36	3.5	287.6	0.96	0.08	good
2004.182	TL05	0.8	124.73	30.3	317.9	90	20	5	297.9	1.2	0.12	good
2004.182	TL14	0.8	124.73	34.6	328.6	90	−2	8	330.6	0.6	0.16	good
2004.252	TL13	33.14	137.2	62.5	359.4	19	23	4	336.4	1.28	0.24	good
2004.259	TL04	14.22	120.41	41	328.7	114	70	8.5	258.7	0.68	0.08	fair
2004.289	TL05	24.53	122.69	51.5	334.4	94	49	12	285.4	1.4	0.24	fair
2004.289	TL07	24.53	122.69	48.9	344.2	94	89	10.5	255.2	1.44	0.28	fair
2004.289	TL09	24.53	122.69	51.3	345.9	94	70	5	275.9	1.12	0.16	good
2004.289	TL12	24.53	122.69	53.3	345.3	94	72	7.5	273.3	1.6	0.24	fair
2004.362	TL07	5.35	94.65	49	300	35	62					null
2004.362	TL14	5.35	94.65	57.2	299.6	35	5	7	294.6	1.16	0.16	fair
2004.362	TL16	12.98	92.39		302.8	23	7	14.5	295.8	0.56	0.12	fair
2005.004	TL16	10.67	92.36	65.4	300.9	23	−87	14.5	387.9	1.32	0.2	fair
2005.024	TL16	7.33	92.48	63.2	298.2	30	−50					null
2005.040	TL12	4.8	95.12	50.6	303.2	44	75	5	228.2	1.52	0.12	fair
2005.089	TL08	2.99	95.4	53.7	294.5	22	−24	3	318.5	1.68	0.12	good
2005.089	TL16	2.99	95.4	58.2	296.6	22	24	1.5	272.6	1.56	0.12	very good
2005.089	TL20	2.99	95.4	58.5	300.8	22	25	5	275.8	2.04	0.44	fair
2005.100	TL08	−1.59	99.7	47.6	292.7	30	72	10.5	220.7	0.68	0.16	good
2005.100	TL12	−1.59	99.7	43	300.8	30	71	3.5	229.8	1.28	0.08	fair
2005.100	TL16	−1.59	99.7	51.9	295.7	30	66	13	229.7	1.44	0.2	fair
					SKIPPY							
1993.163	SA01	51.259	157.692	66.2	9.9	44	−17	1.5	26.9	1.44	0.08	very good
1993.163	SA03	51.259	157.692	72.5	9.8	44	0	8.5	9.8	0.96	0.12	very good
1993.163	SA05	51.259	157.692	75.1	8.7	44	−32					null
1993.163	SA06	51.259	157.692	74.3	6.1	44	−39	8.5	45.1	1.36	0.36	fair
1993.163	SA07	51.259	157.692	77.6	7	44	2	14.5	5	0.76	0.12	fair
1993.232	SA04	21.686	143.064	44.5	3.9	288	−44	16	47.9	0.36	0.08	fair
1993.232	SA05	21.686	143.064	44.6	358.4	288	15					null
1993.244	SA03	−4.331	102.567	42.1	286.7	71	−40	3.5	326.7	0.84	0.08	fair
1993.244	SA05	−4.331	102.567	44.4	288.6	71	11	6.5	277.6	0.72	0.16	fair
1993.321	SB04	1.577	124.033	36.7	323.2	240	67	7.5	256.2	0.84	0.12	fair
1993.333	SB02	10.294	126.477	39.9	334.3	38	57	11.5	277.3	1.32	0.36	fair
1994.220	SC03	24.721	95.2	52.9	320.2	122	73	14.5	247.2	0.68	0.16	good
1994.220	SC05	24.721	95.2	57.3	315.3	122	−50	13	365.3	0.4	0.08	good
1994.220	SC06	24.721	95.2	54.1	322.4	122	75	12.5	247.4	0.44	0.16	fair
1994.253	SC03	7.552	126.599	24.2	353.4	79	−83	4	436.4	1	0.12	good
1994.350	YB01	−3.262	139.842	34.4	343	114	50	10	293	1.68	0.36	fair
1994.350	YB02	−3.262	139.842	34.7	347	114	64	3.5	283	2.32	0.24	fair
1995.019	YB03	−7.395	128.26	33.3	329.4	160	55					null
					WACRATON							
2000.199	WS05	36.283	70.924	75.8	321.9	141	76	8.5	245.9	1	0.16	good
2000.199	WS06	36.283	70.924	75.5	321.6	141	75	17	246.6	0.44	0.16	fair
2000.299	WT05	−6.549	105.63	27.4	331.5	38	82	8.5	249.5	1.8	0.2	good
2000.299	WT08	−6.549	105.63	28.2	327.2	38	68	11	259.2	1.64	0.32	fair
2000.299	WT09	−6.549	105.63	28.5	324.6	38	70	5.5	254.6	1.72	0.16	good
2000.299	WT10	−6.549	105.63	28.6	322.9	38	58	8.5	264.9	1.88	0.24	good

[a]The values correspond to events, Julian date of the event; station, station name; Elat, event latitude; Elon, event longitude; Dist, epicentral distance; Baz, back azimuth; depth, event depth; phi; err_{phi}, error on phi; pol, polarization of the fast shear wave as the back azimuth minus the measured phi; dt; err_{dt}, error on dt; and quality of the measurement.

Of the total number of events considered, 34 have an hypocentral location deeper than 410 km.

4.1.1. Delay Times

[32] For the deep events occurring in the Fiji-Tonga region (Table 1), the delay between the arrival time of the fast and slow S waves is rather small, with an average arithmetic value of 0.88 s. Although this value has no intrinsic significance (hence no computation of associated errors), it highlights the fact that of the 62 measurements considered as reliable, either fair (34) or good (28), only very few might be considered in excess of the continental worldwide average of 1 s obtained from core refracted shear waves. In fact, of the 62 measurements, 19 show a delay time greater than 1 s and one only is in excess of 2 s.

[33] Two deep events (2003.296 and 2004.183, respectively, 503 and 405 km depth) recorded at stations TL02 and TL06, led to values of dt of 2.92 ± 0.24 s and 1.96 ± 0.08 s respectively. The same event (2003.296) recorded at stations TL06 and TL08 highlights a delay time of respectively 0.84 ± 0.16 s and 0.8 ± 0.08 s, whereas event 2004.183 recorded at station TL05 only results in a value of dt of 1 ± 0.16 s. This observation of higher than average delays is therefore very localized and not reproducible at nearby stations; if anisotropy outside the upper mantle has to be invoked to achieve such a high splitting, it needs to be in a very localized region. Thus there does not appear to be large amounts of anisotropy located in the midmantle region or transition zone between Fiji-Tonga and the Australian continent as previously stated [*Wookey and Kendall*, 2004; *Wookey et al.*, 2002].

[34] Intermediate and shallow events, occurring above the 410 km discontinuity, led to substantially higher delay times (1.39 s in average). Taking into account anisotropy potentially due to olivine LPO on the source side, this result is however expected.

4.1.2. Orientation of the Polarization Plane of the Fast S Wave

[35] To the first order, we observe on Figure 5a a rather N-S orientation of the polarization plane of the fast S wave, subparallel to the APM of the Australian plate as defined by various models [*Gripp and Gordon*, 1990, 2002; *Wang and Wang*, 2001]. The APM calculated by the HS3-NUVEL-1A model [*Gripp and Gordon*, 2002] is plotted in Figure 1. However, a closer look at the data reveals a more complex pattern. North of the Flinders ranges, phi tends to be NE-SW, whereas it is oriented NW-SE west of the Eromanga basin. Toward the Gulf of Carpenteria, phi becomes rather N-S again, and it is more NE-SW in the northeastern part of Queensland.

[36] Measurements performed on intermediate and shallow events give more scattered results (see Figure 5b and Table 1): source side contamination is likely to have influenced the results and there is therefore no direct correlation with the orientations of phi measured and the structure of the lithosphere right underneath the seismological station.

4.1.3. Western Australia

[37] A deep event (event 2000.353) recorded at 9 stations constituting part of the WACRATON array in the southern part of the Yilgarn cratonic block, shows an impressive consistency in terms of dt and N-S orientation of phi measured at the seismological stations, over several hundred of kilometers (see Figure 6a).

[38] Considering the intermediate events recorded in western Australia, we also notice (Figure 6a) one event (event 2003.004), recorded at 4 stations located in the central part of the Yilgarn craton, leading to very consistent values of phi ($-74°$ to $-81°$) and dt (1.36 to 1.88 s). Possibly due to source side anisotropy, the delay times are greater than in the case of the deep event.

4.2. Back-Azimuthal Range 280–360°: Java-Sumatra

[39] A total of 115 measurements, classified either good (43), fair (59) or null (13), have been made from 45 events occurring mainly in the Sunda (Java-Sumatra) and Banda arcs. On the total number of events considered, 13 have an hypocentral location deeper than 410 km. The epicentral distance considered as a selection criterion ranges between 24 and 80°; a few events occurring in the Kuril Islands and Japan have therefore also been included in the data set.

4.2.1. Delay Times

[40] An average value of the delay time between the two polarized split S waves of 1.04 s is computed for measurements performed on deep events occurring in the back-azimuthal range 280–360° and recorded at the temporary stations deployed across the Australian continent. 13 out of 45 measurements result in a delay higher than 1 s (Table 2). We note that the highest values of dt have been obtained from the events occurring in Japan and Kuril Islands: their ray paths are longer than for the events occurring in the Java-Sumatra subduction zone, and therefore anisotropy potentially acquired along the ray path could contribute to higher delays. Measurements performed on intermediate and shallow events, for which the source side anisotropy related to olivine LPO above the 410 km discontinuity is not avoided, result in higher delays: 32 out of 70 values are over 1 s for an average arithmetic value of 1.17 s.

4.2.2. Orientation of the Polarization Plane of the Fast S Wave

[41] Measurements performed on deep events give rather scattered results (Figure 7a and Table 2). The orientation of

Figure 5. Plot of good (black lines) and fair (grey lines) measurements performed on (a) deep and (b) shallow and intermediate events occurring in the Fiji-Tonga subduction zone. The orientation of the line is parallel to the orientation of the polarization plane of the fast S wave and its length is proportional to the delay time. The names of some geographical locations discussed in the text are indicated. Figures 5c and 5d correspond to a zoom on eastern Australia. (c) Results from shear wave splitting measurements performed on direct S waves from deep events are superimposed on the latest surface wave tomographic model at 200 km depth (S. Fishwick, personal communication, 2005). (d) Geological TL as defined by *Scheibner* [1974] superimposed to the results of shear wave splitting measurements performed on deep event. We chose this definition of the geological TL for comparison with *Clitheroe and van der Hilst* [1997] and *Heintz and Kennett* [2005] previous studies dealing with core refracted shear waves and comparing the orientations of phi with the above mentioned geological TL.

the polarization plane of the fast S wave does not seem to be parallel to the APM of the Australian plate (see Figure 1 for comparison), nor to local structural trends. We however notice a slightly NW-SE orientation of phi toward the Gulf of Carpenteria, whereas phi is more oriented NE-SW in the northeastern part of Queensland.

[42] A deep event occurring in the Kuril Islands region (event 2003.208, mean back azimuth: 0°) leads to rather consistent values of phi oriented N25°W across several stations from the TASMAL deployment (TL04, TL06, TL10, TL11, TL13 and TL16). A deep event occurring in the Philippines subduction zone (event 2003.182, mean

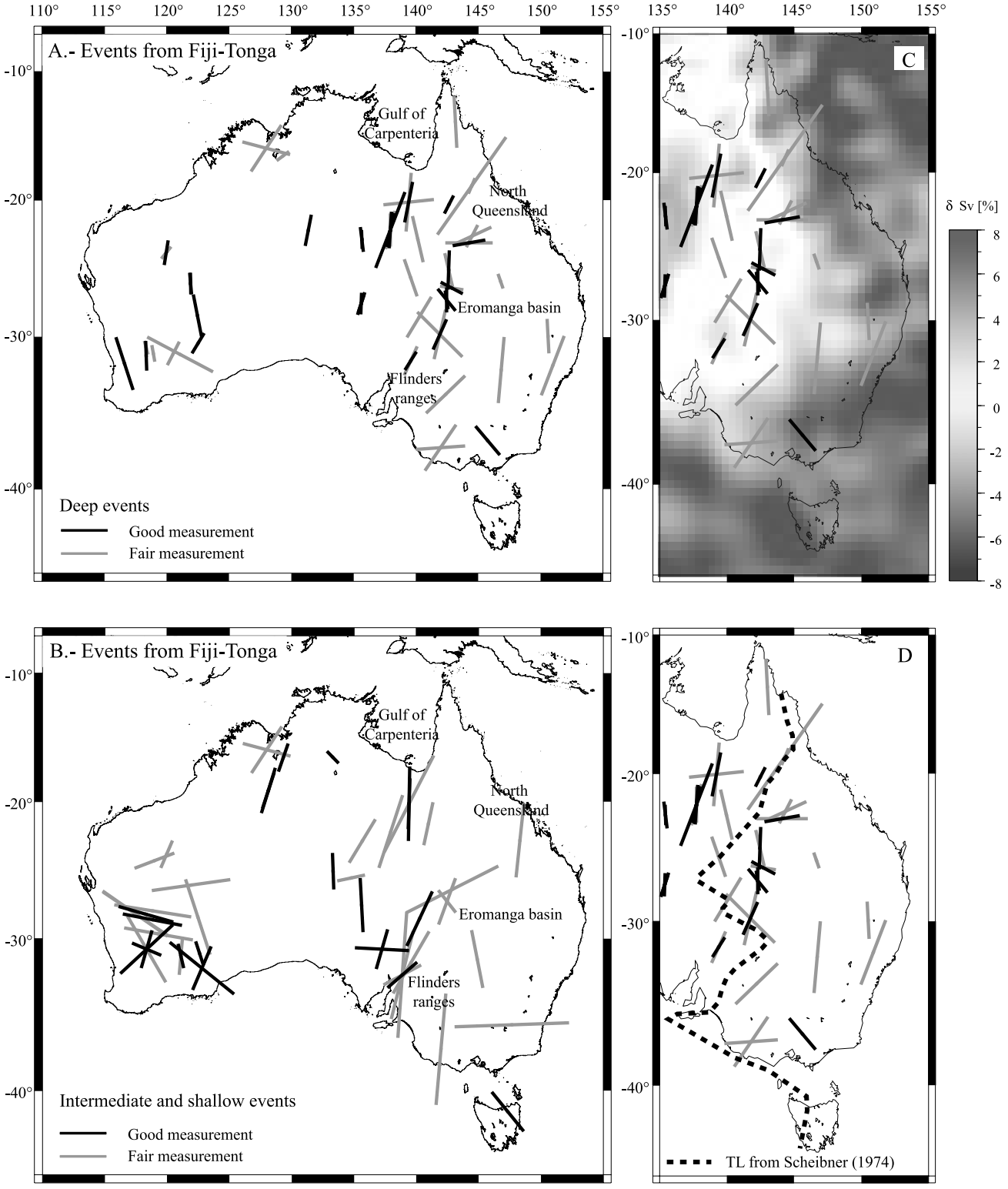

Figure 5

back azimuth: 320°) and recorded at stations TL01, TL02, TL03, TL04, TL05 and TL06, leads to coherent values of phi roughly oriented N25°E. A back-azimuthal variation in terms of the anisotropic parameters measured is therefore observed.

[43] Measurements performed on intermediate and shallow events are plotted in Figure 7b. A rather consistent NE-SW orientation of phi is observed in the western part of the continent, west of 140° longitude.

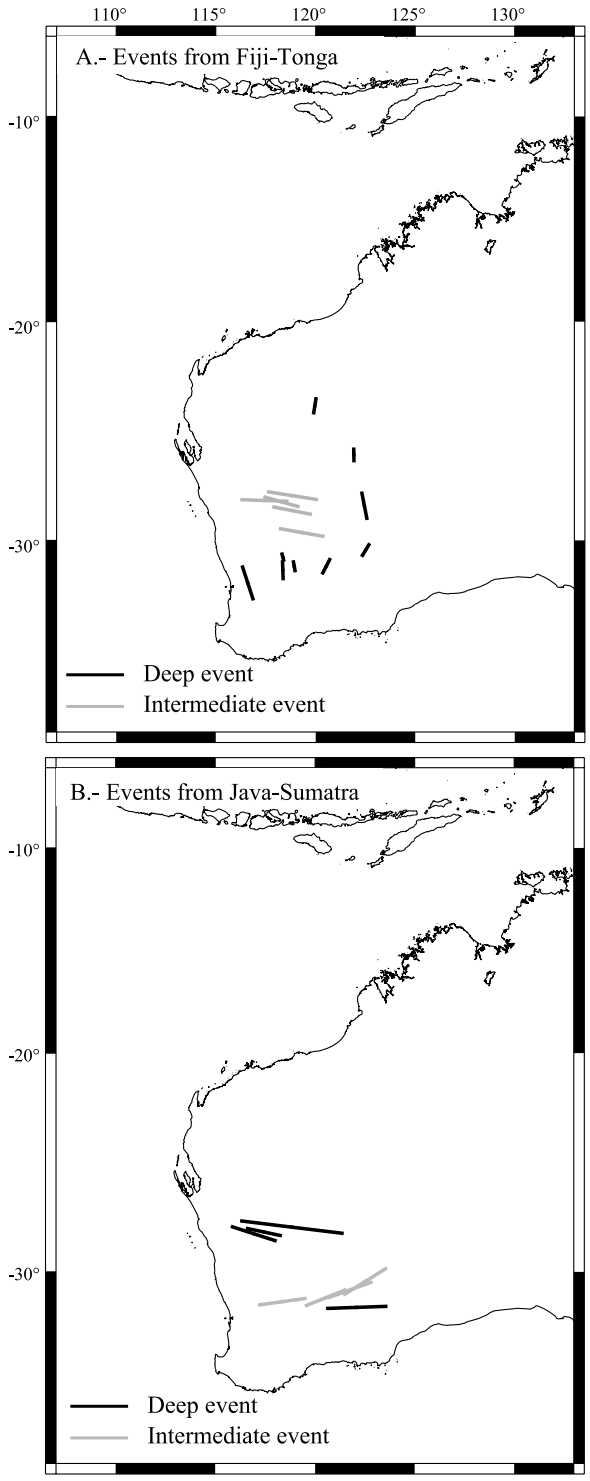

4.2.3. Western Australia

[44] A deep event (event 2003.017) recorded at 4 stations deployed within the framework of the WACRATON experiment results in consistent E-W orientation of the polarization plane of the fast S wave (Figure 6b). The values of dt associated with these measurements are well over 1 s but incoherent between the stations. On the other hand, a shallow event (event 2000.299) recorded at another set of 4 stations in western Australia highlights an average value of phi oriented N70°E, and a consistent 1.7 s of delay between the arrival of the fast and slow split S waves (Figure 6b).

5. Discussion

5.1. Delay Times: Evidence for Midmantle Deformation?

[45] From my measurements of delay times at the temporary stations deployed across the continent, I do not have any evidence for the existence of midmantle deformation associated with anisotropy in the lower mantle between Fiji-Tonga and the Australian continent in contrast to [*Wookey and Kendall*, 2004; *Wookey et al.*, 2002]. Measurements performed on events occurring in the deep part of the Java-Sumatra subduction zones also do not require mid to lower mantle anisotropy. The average values obtained for dt (respectively 0.88 s and 1.04 s for each data set) can be achieved with a standard upper mantle anisotropy of ~5%, in a ~100 km thick lithosphere. For the higher dt measured and related to deep events, a slight asthenospheric contribution might be required to explain 1–2 s delay in the eastern part of the continent, but there is no need for an anisotropic mid to lower mantle to explain the present results.

[46] In the western part of the continent, tomographic studies [*Debayle and Kennett*, 2000b; *Fishwick et al.*, 2005; *Kennett et al.*, 2004b; *Simons et al.*, 1999] suggest a 200–250 km thick cratonic lithosphere. Considering 5% as a standard value of intrinsic anisotropy in the lithospheric upper mantle, this could lead to a delay between the fast and slow split S wave up to 2.1–2.7 s, from the lithospheric contribution alone.

Figure 6. Example of the consistency in terms of the anisotropic parameters computed at stations located in western Australia for four different events. The orientation of each line is parallel to the orientation of the polarization plane of the fast S wave, and its length is proportional to the delay between the arrival time of the fast and slow components. (a) Comparison between the orientation of the polarization plane of the fast S wave measured at different stations in western Australia from one deep event (event 2000.353, 628 km depth), black lines, and one intermediate event (event 2003.004, 378 km depth), grey lines, occurring in the Fiji-Tonga subduction zone. (b) Comparison between the orientation of the polarization plane of the fast S wave measured at different stations in western Australia from one deep event (event 2003.017, 483 km depth), black lines, and one intermediate event (event 2000.299, 38 km depth), grey lines, occurring in the Java-Sumatra subduction zone.

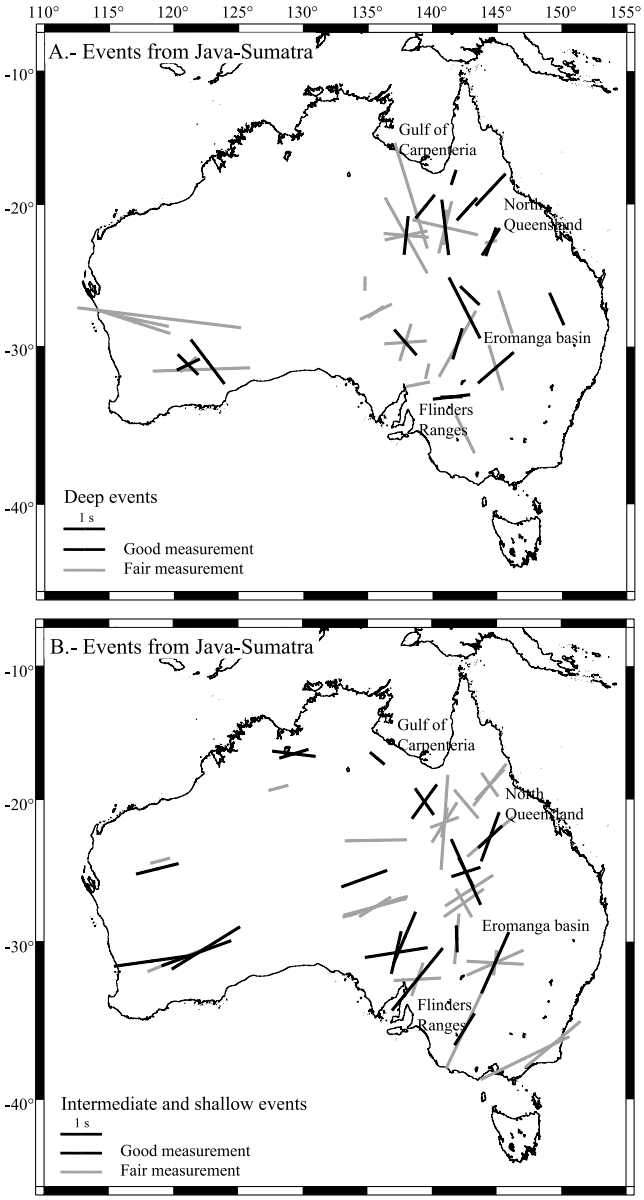

Figure 7. Plot of good (black lines) and fair (grey lines) measurements performed on (a) deep and (b) shallow and intermediate events occurring in the Java-Sumatra subduction zone. The deep events occur below 410 km depth, whereas the shallow and intermediate events have a hypocenter located between 14 and 409 km depth. The orientation of the line is parallel to the orientation of the polarization plane of the fast S wave, and its length is proportional to the delay time. The names of some geographical locations discussed in the text are indicated.

[47] After reanalysis of the initial data in view of the potential existence of large amplitude shear coupled P waves leading to a mixture of direct SV and shear coupled P waves that might be interpreted as pure SV motion [*Saul and Vinnik*, 2002], the reprocessed data set of *Wookey and Kendall* [2004] consists of 30 high-quality estimates, performed on 26 events deeper than 300 km occurring in the Fiji-Tonga subduction zone and recorded at Australian permanent stations. Only one measurement performed on a deep event recorded at station NWAO highlights a dt of 6.2 s, whereas all the other values are below 3.55 s. NWAO is located in southwestern Australia; ray paths from events occurring in the Fiji-Tonga subduction zone and reaching NWAO travel therefore a large portion in the lower mantle and measuring the highest dt at NWAO could be expected in the case of a mid to low-mantle contribution.

[48] The depth criterion of 300 km used by *Wookey and Kendall* [2004] and *Wookey et al.* [2002] leaves a few events located above the olivine-spinel phase transition depth for which source side contamination might not be avoided, leading therefore to high delay times that cannot be reasonably compared with the present data set.

[49] Despite the decrease of the splitting values after reanalysis of the data set, and the possible source side contribution, *Wookey and Kendall* [2004] maintain the hypothesis that significant anisotropy is present in the midmantle region between Fiji-Tonga and the Australian continent. Taking into account the direct S phase only and without filtering the signal, I however confirm in my data set average values of dt, oscillating around the 1 s worldwide average [*Silver*, 1996] for truly deep sources, below 410 km depth.

[50] *Wookey et al.* [2002] reported a minimum splitting for events occurring at ~23°S latitude, confirmed by *Wookey and Kendall* [2004]. They correlated this observation with the transition between the Tonga and Kermadec subducting slabs at ~25°S latitude [*Hamburger and Isacks*, 1987]. Despite having overall smaller dt values than *Wookey and Kendall* [2004] and *Wookey et al.* [2002], I notice minimum values of dt (from 0.36 to 0.92 s) measured for events occurring between 23 and 25°S latitude with respect to surrounding events, with a delay of e.g., 1.96 s for a latitude of 25.54°S (see square on Figure 8). However, a similar observation can be made for events occurring between 19 and 21°S latitude, without any obvious correlation with the morphology of the subducting plate. I therefore cannot highlight any correlation between the measured splitting values and the change of morphology of the subducting Pacific plate around 25°S latitude. An even more comprehensive data set is needed to make such a statement.

5.2. Comparison Between Measurements Performed on SKS and Direct S Phases

[51] Previous studies [*Clitheroe and van der Hilst*, 1997; *Heintz and Kennett*, 2005] based on an average of 6 months of core refracted shear waves recording, suggest a rather complex pattern of seismic anisotropy at the continental scale, not obviously correlated with the APM. Relationships between phi and structural trends can be highlighted in some places, suggesting anisotropy frozen in the lithosphere. Along the poorly constrained TL, directions of anisotropy measured at some stations located in the close vicinity of the TL as defined by *Scheibner* [1974] appear to exhibit a curvilinear trend somewhat similar to that of this geological TL.

[52] Regarding the data obtained from 2 years of recording at the TASMAL stations from core refracted shear waves, we now observe apparent isotropy in the Australian upper mantle underneath numerous seismological stations [*Heintz and Kennett*, 2006].

[53] Considering measurements performed on direct S waves from deep events occurring in the Fiji-Tonga sub-

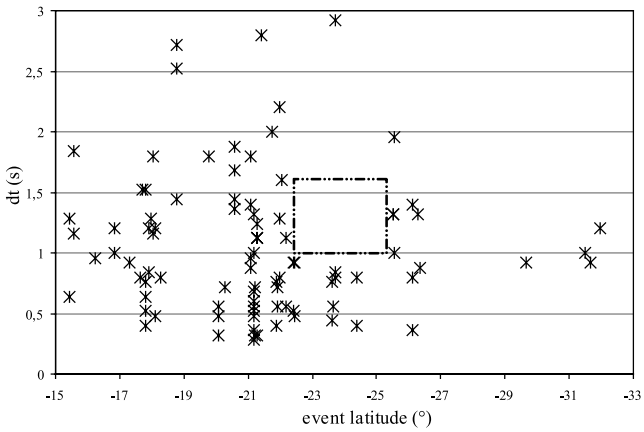

Figure 8. Delay times versus event latitude for fair and good measurements performed on deep and shallow and intermediate events occurring in the Fiji-Tonga subduction zone. The box defines the minimum values of dt (from 0.36 to 0.92 s) measured for events occurring between 23 and 25°S latitude in order to compare with a statement enounced by *Wookey et al.* [2002] and confirmed by *Wookey and Kendall* [2004]. They reported a minimum splitting for events occurring at ~23°S latitude and correlated this observation with the transition between the Tonga and Kermadec subducting slabs at ~25°S latitude [*Hamburger and Isacks*, 1987].

duction zone, some orientations of phi measured at a few stations located in the near vicinity of the geological TL as defined by *Scheibner* [1974] may exhibit a local parallelism with the trend of the TL (see Figure 5d). Some stations appear to be very well constrained as far as the orientation of the polarization plane of the fast S wave is concerned, and TL06 is the best example: 10 measurements performed on various events lead to an average phi of 15°. Considering the numerous versions of the TL [*Gunn et al.*, 1997; *Hill*, 1951; *Scheibner*, 1974; *Shaw et al.*, 1996; *Veevers and Powell*, 1984], their various interpretations, and the high controversy around the TL concept, it is not surprising that no clear correlation is seen across the whole continent.

[54] In Figure 5c, I superimpose on my measurements the latest tomographic results obtained at 200 km depth (S. Fishwick, personal communication, 2005). The successive orientations of the polarization plane of the fast S wave as deduced from measurements performed on the deep events occurring in the Fiji-Tonga subduction zone at different portable stations lead to a curve that, in some local places, show a reasonable correlation with the transition from fast to slow shear wave speeds (i.e., the tomographic TL).

[55] Despite more scattered results obtained for measurements performed on deep events occurring in the back-azimuthal range 280–360°, a similar trend is observed in this set of results: an ENE-WSW orientation of the polarization plane of the fast S wave is observed east of the Flinders ranges, whereas it becomes NW-SE north of this region to be finally N-S toward the Gulf of Carpenteria and more NE-SW in the northern part of Queensland (Figure 7a).

[56] While locally there are some correlations, any parallelism at the scale of the eastern part of the continent (from northern Queensland to southern Victoria) between the shape of the geological and/or tomographic TL and the orientation of phi obtained through measurements performed on either core refracted shear waves or direct S waves, is rather difficult to establish.

[57] The comparison between seismic anisotropy measurements obtained from core refracted shear waves [*Heintz and Kennett*, 2005] and direct S waves gives however important information regarding the structure of the upper mantle underneath the Australian continent. We can generalize to the continental scale an observation previously made at the permanent stations only: measurements performed on core refracted shear waves indicate apparent isotropy [*Heintz and Kennett*, 2006] whereas measurements performed on direct S waves show clear evidence of anisotropy.

5.3. How to Reconcile the Apparent Lack of SKS Splitting and the Distinct Direct S Splitting?

[58] Transverse anisotropy with a vertical axis of symmetry would be manifested by a difference between horizontally (SH) polarized versus vertically (SV) polarized waves. To express the polarization of the fast S phase in comparison to the SV or SH (radial or transverse) directions, I subtract the measured phi from the back azimuth of the event. This value is called "pol" in Tables 1 and 2. A pol of 90° is SH polarized, whereas 0° is SV polarized. This helps to find out which component of the S wave is actually the fastest and therefore gives some hints about the symmetry of the anisotropic medium.

[59] After reanalysis of their data set, *Wookey and Kendall* [2004] calculated an average fast direction in the SV/SH coordinate system of 84.2 ± 23° compared to the previous value of 111 ± 31° computed by *Wookey et al.* [2002]. They interpreted their results in terms of a general trend of SH leading SV, suggesting a roughly vertically oriented transverse isotropic medium, consistent with the lack of SKS shear wave splitting observed at the Australian permanent stations.

[60] Following this procedure, I calculated the polarization of the fast S phase in the SV/SH coordinate system for my data set. The results are presented in Figure 9 and Table 1. My results corroborate the results of *Wookey et al.* [2002] and *Wookey and Kendall* [2004], showing a general trend of SH leading SV, with an average fast direction trending 89.88 ± 18.96°. These values correspond to the mean and average deviation of a distribution computed with a simple Monte Carlo integration on randomly generated points with a normal (Gaussian) distribution. In this case we consider each value of pol distributed along a Gaussian, the associated errors being one standard deviation. This result is in good agreement with *Debayle and Kennett* [2000a], recovering anisotropy in the Australian upper mantle from Love and Rayleigh waveform inversion. This study highlighted a polarization anisotropy with SH faster than SV in the upper 200–250 km of the mantle for most of Australia. The existence of a vertically oriented transverse isotropic medium might therefore be considered as a plausible explanation to reconcile the lack of SKS splitting with the non negligible direct S wave splitting observed at the temporary stations.

5.4. West Australian Craton

[61] The consistency in terms of dt and N-S orientation of phi measured at 9 stations belonging to the southern part of

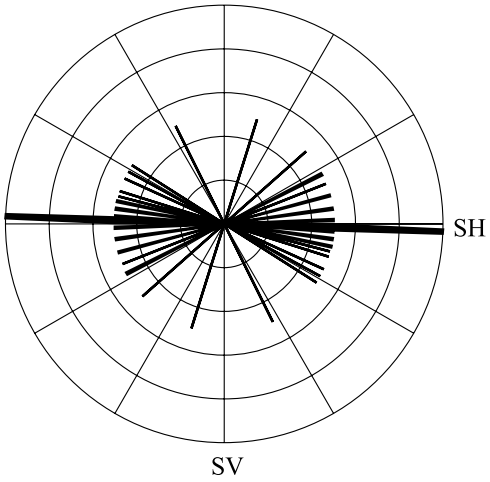

Figure 9. Polar histogram of the orientation of the polarization plane of the fast shear wave. Only good results from deep events are considered. The average polarization is 89.88°, showing a general trend of SH leading SV.

the WACRATON array, for one deep event from the Fiji-Tonga subduction zone (event 2000.353, 628 km depth), is a well constrained result (Figure 6a). A similar coherence has been obtained through core refracted shear wave measurement [*Heintz and Kennett*, 2005] in the same area, extending over 600 km.

[62] A deep event occurring in the Java-Sumatra subduction zone (event 2003.017, 483 km depth) also results in very consistent values of phi, oriented E-W, measured at 4 stations deployed across the western Australian craton, along a N-S profile (Figure 6b).

[63] Considering these events occur below 410 km depth, and thereby avoiding as far as possible the source side contamination in the results, we end up with a rather straightforward picture: events from the Fiji-Tonga subduction zone recorded at stations deployed in western Australia highlight a N-S direction of phi, whereas deep events from the Java-Sumatra subduction zone, recorded in the same region, suggest an E-W orientation of the polarization plane of the fast S wave. As the initial polarization is an unknown, it is therefore difficult to account for a back-azimuthal variation of phi that could be explained by a two-layer system underneath the western part of the continent.

[64] However, these various observations lead to the conclusion that the lithosphere underneath the Yilgarn craton in western Australia is laterally very homogeneous over several hundred of kilometers. Such a consistency might appear as a characteristic feature of old cratonic blocks. The same result has previously been observed for the Canadian [*Silver and Kaneshima*, 1993], South African [*Silver et al.*, 2001] and Arabian [*Wolfe et al.*, 1999] shields.

6. Conclusion

[65] Shear wave splitting measurements have been performed on deep events occurring in the Fiji-Tonga subduction zone recorded at temporary stations deployed across the Australian continent. A careful analysis of the data with regard to the effects of filtering, windowing and contamination of the coda of the direct S waves by shear coupled P or PcS waves, provides a comprehensive and well constrained data set. The overall measurements performed highlight an average arithmetic value of 0.9 s for the delay time between the arrival of the fast and slow S waves. I therefore do not have any evidence in my data set for the existence of midmantle deformation between Fiji-Tonga and Australia as suggested by previous studies dealing with similar events recorded at the five permanent stations spread across the continent. The results from deep events occurring in the Java-Sumatra subduction zone and recorded at the same stations, slightly complicate the pattern of anisotropy in terms of the orientation of the polarization plane of the fast S waves, but an average delay of 1.04 s does not require midmantle deformation in the mantle north of the Australian continent to be explained.

[66] The apparent isotropy measured on core refracted shear waves recorded at the temporary stations can be reconciled with the noticeable anisotropy deduced by analysis of direct S waves with a vertically oriented transverse isotropic medium; a general trend of SH leading SV reinforces this hypothesis.

[67] At stations deployed in western Australia, the consistency over several hundred of kilometers in terms of the orientation of the polarization plane of the fast S wave suggests a very coherent lithospheric structure underneath the Yilgarn craton. This might appear as a characteristic feature of old cratonic blocks, as the same results have previously been observed for the Canadian, South African and Arabian shields.

[68] **Acknowledgments.** I would like to thank all the various people who have been involved in data collection over the years at the Research School of Earth Sciences, Australian National University, and Armando Arcidiaco for data handling. I am very grateful to Martha Savage and Vadim Levin for very useful and constructive reviews. Many thanks also to Brian Kennett and Stewart Fishwick for useful discussion and to James Wookey for providing me with his table of results.

References

Barruol, G., and R. Hoffmann (1999), Upper mantle anisotropy beneath Geoscope stations, *J. Geophys. Res.*, *104*(B5), 10,757–10,773.

Betts, P. G., D. Giles, G. S. Lister, and L. R. Frick (2002), Evolution of the Australian lithosphere, *Aust. J. Earth Sci.*, *49*, 661–695.

Chen, W.-P., and M. R. Brudzinski (2003), Seismic anisotropy in the mantle transition zone beneath Fiji-Tonga, *Geophys. Res. Lett.*, *30*(13), 1682, doi:10.1029/2002GL016330.

Clitheroe, G., and R. D. van der Hilst (1997), Complex anisotropy in the Australian lithosphere from shear-wave splitting in broad-band SKS records, in *Structure and Evolution of the Australian Continent*, *Geodyn. Ser.*, vol. 26, edited by J. Braun et al., pp. 73–78, AGU, Washington, D. C.

Debayle, E., and B. L. N. Kennett (2000a), Anisotropy in the Australasian upper mantle from Love and Rayleigh waveform inversion, *Earth Planet. Sci. Lett.*, *184*, 339–351.

Debayle, E., and B. L. N. Kennett (2000b), The Australian continental upper mantle: Structure and deformation inferred from surface waves, *J. Geophys. Res.*, *105*(B11), 25,423–25,450.

Direen, N. G., and A. J. Crawford (2003), The Tasman Line: Where is it, what is it, and is it Australia's Rodinian breakup boundary?, *Aust. J. Earth Sci.*, *50*, 491–502.

Fischer, K. M., and D. A. Wiens (1996), The depth distribution of mantle anisotropy beneath the Tonga subduction zone, *Earth Planet. Sci. Lett.*, *142*, 253–260.

Fishwick, S., B. L. N. Kennett, and A. M. Reading (2005), Contrasts in lithospheric structure within the Australian craton—Insights from surface wave tomography, *Earth Planet. Sci. Lett.*, *231*, 163–176.

Gorbatov, A., and B. L. N. Kennett (2003), Joint bulk-sound and shear tomography for western Pacific subduction zones, *Earth Planet. Sci. Lett.*, *210*, 527–543.

Gripp, A. E., and R. G. Gordon (1990), Current plate velocities relative to the hotspots incorporating the NUVEL-1 global plate motion model, *Geophys. Res. Lett.*, *117*(8), 1109–1112.

Gripp, A. E., and R. G. Gordon (2002), Young tracks of hotspots and current plate velocities, *Geophys. J. Int.*, *150*, 321–361.

Gunn, P. J., P. Milligan, T. Mackey, S. Liu, A. Murray, D. Maidment, and R. Haren (1997), Geophysical mapping using the national airborne and gravity datasets: An example focusing on Broken Hill, *J. Aust. Geol. Geophys.*, *17*, 127–136.

Hamburger, M. W., and B. L. Isacks (1987), Deep earthquakes in the southwest Pacific: A tectonic interpretation, *J. Geophys. Res.*, *92*(B13), 13,841–13,854.

Heintz, M., and B. L. N. Kennett (2005), Continental scale shear wave splitting analysis: Investigation of seismic anisotropy underneath the Australian continent, *Earth Planet. Sci. Lett.*, *236*, 106–119.

Heintz, M., and B. L. N. Kennett (2006), The apparently isotropic Australian upper mantle, *Geophys. Res. Lett.*, *33*, L15319, doi:10.1029/2006GL026401.

Hill, D. (1951), Geology, in *Handbook of Queensland*, edited by G. Mack, pp. 13–24, Aust. Assoc. for the Adv. Sci., Brisbane.

Kendall, J.-M., and P. G. Silver (1996), Constraints from seismic anisotropy on the nature of the lowermost mantle, *Nature*, *381*, 409–412.

Kennett, B. L. N., and E. R. Engdahl (1991), Travel times for global earthquake location and phase identification, *Geophys. J. Int.*, *105*, 429–465.

Kennett, B. L. N., S. Fishwick, and M. Heintz (2004a), Lithospheric structure in the Australian region—A synthesis of surface wave and body wave studies, *Explor. Geophys.*, *35*, 242–250.

Kennett, B. L. N., S. Fishwick, A. M. Reading, and N. Rawlinson (2004b), Contrasts in mantle structure beneath Australia—Relation to Tasman lines?, *Aust. J. Earth Sci.*, *51*, 563–569.

Myers, J. S., R. D. Shaw, and I. M. Tyler (1996), Tectonic evolution of Proterozoic Australia, *Tectonics*, *15*(6), 1431–1446.

Ozalaybey, S., and W.-P. Chen (1999), Frequency-dependent analysis of SKS/SKKS waveforms observed in Australia: Evidence for null birefringence, *Phys. Earth Planet. Inter.*, *114*(3–4), 197–210.

Puspito, N. T., Y. Yamanaka, T. Miyatake, K. Shimazaki, and K. Hirahara (1993), Three-dimensional P-wave velocity structure beneath the Indonesian region, *Tectonophysics*, *220*(1–4), 175–192.

Saul, J., and L. P. Vinnik (2002), Mantle deformation or processing artefact?, *Nature*, *422*, 136.

Savage, M. K. (1999), Seismic anisotropy and mantle deformation: What have we learned from shear wave splitting?, *Rev. Geophys.*, *37*(1), 65–106.

Scheibner, E. (1974), Fossil fracture zones (transform faults), segmentation and correlation problems in the Tasman Fold Belt System, in *The Tasman Geosynclin—A Symposium in Honour of Professor Dorothy Hill*, edited by A. K. Denmead, G. W. Tweedale, and A. F. Wilson, pp. 65–96, Queensl. Div., Geol. Soc. of Aust., Brisbane.

Shaw, R. D., P. Wellman, P. J. Gunn, A. J. Whitaker, C. Tarlowski, and M. P. Morse (1996), Guide to using the Australian crustal elements map, *Rec. 1996*(30), Aust. Geol. Surv. Org., Canberra.

Silver, P. G. (1996), Seismic anisotropy beneath the continents: Probing the depths of Geology, *Annu Rev. Earth Planet. Sci.*, *24*, 385–432.

Silver, P. G., and W. W. Chan (1991), Shear wave splitting and subcontinental mantle deformation, *J. Geophys. Res.*, *96*(B10), 16,429–16,454.

Silver, P. G., and S. Kaneshima (1993), Constraints on mantle anisotropy beneath precambrian North America from a transportable teleseismic experiment, *Geophys. Res. Lett.*, *20*(12), 1127–1130.

Silver, P. G., S. Gao, K. H. Liu, and Kaapvaal Seismic Group (2001), Mantle deformation beneath southern Africa, *Geophys. Res. Lett.*, *28*(13), 2493–2496.

Simons, F. J., A. Zielhuis, and R. D. van der Hilst (1999), The deep structure of the Australian continent from surface wave tomography, *Lithos*, *48*, 17–43.

van der Hilst, R. D. (1995), Complex morphology of subducted lithosphere in the mantle beneath the Tonga trench, *Nature*, *374*, 154–157.

van der Hilst, R., B. Kennett, D. Christie, and J. Grant (1994), Project Skippy explores the lithosphere and mantle beneath Australia, *Eos Trans. AGU*, *75*(15), 177, 180–181.

Veevers, J. J., and C. M. Powell (1984), Epi-adelaidean: Regional shear, in *Phanerozoic Earth History of Australia*, edited by J. J. Veevers, pp. 278–284, Clarendon, Oxford, U. K.

Vinnik, L. P., L. I. Makeyeva, A. Milev, and A. Y. Usenko (1992), Global patterns of azimuthal anisotropy and deformations in the continental mantle, *Geophys. J. Int.*, *111*, 433–447.

Wang, S., and R. Wang (2001), Current plate velocities relative to hotspots: Implications for hotspot motion, mantle viscosity and global reference frame, *Earth Planet. Sci. Lett.*, *189*, 133–140.

Widiyantoro, S., and R. D. van der Hilst (1996), Structure and evolution of the lithospheric slab beneath the Sunda arc, Indonesia, *Science*, *271*, 1566–1570.

Widiyantoro, S., and R. D. van der Hilst (1997), Mantle structure beneath Indonesia inferred from high resolution tomographic imaging, *Geophys. J. Int.*, *130*, 167–182.

Widiyantoro, S., B. L. N. Kennett, and R. D. van der Hilst (1999), Seismic tomography with P and S data reveals lateral variations in the rigidity of deep slabs, *Earth Planet. Sci. Lett.*, *173*, 91–100.

Wolfe, C. J., F. L. Vernon III, and A. Al-Amri (1999), Shear-wave splitting across western Saudi Arabia: The pattern of upper mantle anisotropy at a Proterozoic shield, *Geophys. Res. Lett.*, *26*(6), 779–782.

Wookey, J., and J.-M. Kendall (2004), Evidence of midmantle anisotropy from shear wave splitting and the influence of shear-coupled *P* waves, *J. Geophys. Res.*, *109*, B07309, doi:10.1029/2003JB002871.

Wookey, J., J.-M. Kendall, and G. Barruol (2002), Mid-mantle deformation inferred from seismic anisotropy, *Nature*, *415*, 777–780.

M. Heintz, Research School of Earth Sciences, Australian National University, Mills Road, Canberra, ACT 0200, Australia. (maggy@rses.anu.edu.au)